Rensselaer

Richard T. Lahey, Jr.
Edward E. Hood, Jr. Professor of Engineering

October 31, 1993

Dr. Edwin P. Rood
Scientific Officer Code: 1132F
Office of Naval Research
800 North Quincy Street
Arlington, VA 22217-5000

Dear Dr. Rood:

The purpose of this letter is to transmit the eleventh quarterly report for ONR Grant N00014-91-J-1271, "An Experimental Study of Plunging Liquid Jet Induced Air Carryunder and Dispersion," (Lahey & Drew - Co-PI).

During this report period the analysis of the pool surface depression by the plunging liquid jet (which leads to the entrainment of air) was completed. This has resulted in a technical paper entitled, "An Analysis of Pool Surface Deformation Due to a Plunging Liquid Jet. This paper will be submitted to the *Journal of Fluid Mechanics* (JFM) for archival publication.

We are continuing our CFD analysis of the plunging liquid jet data we have taken. In particular, a more generalized two-fluid model is being coped. Moreover, in the future we plan to analyze the two-phase shear flow data of Professor J. Lasheras (UC-SD) once it is available to us.

If you need any further information concerning this report please don't hesitate to contact me [(518) 276-8579] or Professor Drew [(518) 276-6903].

Sincerely yours,

R T Lahey Jr

Dr. R.T. Lahey, Jr.
The Edward E. Hood, Jr. Professor of Engineering

RTL/ev
Enclosure

cc: Administrative Grants Officer
Director, Naval Research Laboratory
Defense Technical Information Center
D.A. Drew
F. Bonetto

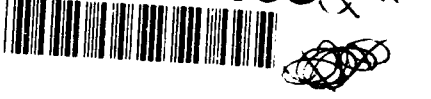

AN ANALYSIS OF POOL SURFACE DEFORMATION DUE TO A PLUNGING LIQUID JET

F. Bonetto
D.A. Drew
R.T. Lahey, Jr.
Center for Multiphase Research
Rensselaer Polytechnic Institute
Troy, NY 12180-3590 USA

ABSTRACT

When a liquid jet impacts a pool containing the same liquid and surrounded by a still gas, a surface depression is produced. The surface shape is determined by the Weber number, $We = \frac{\frac{1}{2}\rho_\ell V_\ell^2 x_o}{\sigma}$ and the Bond number, $B_o = \frac{\rho_\ell g x_o}{\sigma}$. In this work the shape of the surface is obtained as a function of the Weber number and Bond number by using a non-singular perturbation technique.

INTRODUCTION

The entrainment of non-condensible gases by a plunging liquid jet impacting a liquid pool is important for some practical problems. For example, the absorption of greenhouse gases into the ocean has been hypothesized to be highly dependent upon the air carryunder that occurs during breaking waves, which represent a type of plunging liquid jet [Monahan, 1991; Kerman, 1984]. Other applications include some type of liquid/gas chemical reactors. In order to enhance the reaction rate, a jet of liquid entrains the surrounding gas reactant forming a bubbly two-phase jet. The reaction rate is enhanced because of the increase of the interfacial area density and the pseudo-turbulence produced by the entrained gas bubbles.

Other less obvious applications are associated with the dynamics of the slug flow regime in two-phase flow. For example, in vertical slug flow, the Taylor bubbles move upward with an almost constant velocity. The liquid film

surrounding the Taylor bubbles drains downward forming an annular liquid jet. Therefore, a gas entrainment problem, similar to the one studied in this work, occurs behind the Taylor bubbles. In particular, a Kelvin-Helmholtz instability occurs at the interface in the rear portion of the Taylor bubble such that small gas bubbles are entrained into the liquid plug behind the Taylor bubble.

DISCUSSION

Most prior theoretical studies were done for liquid jets with very low liquid velocities, and had applications for fiber coating, etc. Lezzi & Prosperetti [1991] performed a stability analysis of the gas entrained by a plunging liquid jet by assuming the liquid jet and the pool to be inviscid liquids and the gas to be viscous. They did not analyze the surface depression.

Bonetto, et al [1993] analyzed an inclined plunging liquid jet. They assumed that both the gas and the liquid were inviscid and they obtained the entrained gas flow rate. The volumetric flow rate of entrained gas is one of the most important quantities which one wants to compute in problems of this type. The key parameter in such evaluations is the gas gap thickness (ie, the shape of the induced surface depression).

The objective of this work was to evaluate the induced surface depression caused by a plane plunging liquid jet. We have assumed that both fluids are inviscid and irrotational, and that the gas region is at constant pressure. Hence the appropriate equation for this problem is Laplace's equation for the liquid and the associated interfacial jump condition. The problem may be described by two parameters, the Weber number, $We = \frac{\frac{1}{2}\rho_\ell V_\ell^2 x_o}{\sigma}$, and the Bond number, $B_o = \frac{\rho_\ell g x_o}{\sigma}$, where x_o is the half-width of the plunging liquid jet, V_ℓ is the velocity of the liquid

jet, ρ_ℓ is the density of the liquid, g is the gravitational acceleration, and σ is the surface tension.

We have used a nonsingular perturbation technique to solve the problem. That is, we have expanded the solutions for relatively small We number, and substitute these expressions into Laplace's equation and the interfacial jump condition. Equating terms of the same order in We, one obtains a recursive system of equations, which we have solved numerically up to third order.

ASYMPTOTIC EXPANSION

The purpose of this section is to compute the position of the interface, $\hat{y} = \hat{\eta}(\hat{x})$ (shown schematically in Figure-1).

For the assumption of irrotational, inviscid flow the governing equations for the liquid field are,

$$\nabla^2 \hat{\psi} = 0 \tag{1}$$

where $\hat{\psi}$ is the stream function. The two velocity components are then given as,

$$\hat{u} = \frac{\partial \hat{\psi}}{\partial \hat{y}} \tag{2}$$

$$\hat{v} = -\frac{\partial \hat{\psi}}{\partial \hat{x}} \tag{3}$$

where $\hat{u}$ and $\hat{v}$ are the velocity components along the $\hat{x}$ and $\hat{y}$ axis, respectively. If we prescribe a value of $\hat{\psi}$, or its derivative normal to the surface, $\frac{\partial \hat{\psi}}{\partial \hat{n}}$, for every point on the boundary, we have a well-posed problem. As shown in Fig.-2, the plane $\hat{x} = 0$ is a symmetry plane. Then the transverse lateral velocity, $\hat{u}$ must vanish for every $\hat{y}$ at $\hat{x} = 0$. That is, from Eq. (2)

$$\hat{u}(\hat{x} = 0, \hat{y}) = \frac{\partial \hat{\psi}}{\partial \hat{y}} (\hat{x} = 0, \hat{y}) = 0 \tag{4}$$

on the centerline of the plunging liquid jet. We know that the axial velocity must be V_ℓ at points where the jet is impacting. From Fig-1 and Eq. (3), we see that:

$$\hat{v}\ (0 < \hat{x} < x_o, \hat{y} = 0) = - \frac{\partial \hat{\psi}}{\partial \hat{x}} (0 < \hat{x} < x_o, \hat{y} = 0) = V_\ell \tag{5}$$

For $\hat{x} > x_o$, the free surface position, $\hat{\eta}(\hat{x})$, must be coincident with a streamline. Without loss of generality, we make the free surface coincident with the streamline $\hat{\psi} = 0$. Then,

$$\hat{\psi}\left(\hat{x}, \hat{\eta}(\hat{x})\right) = 0 \tag{6}$$

We assume that the pressure in the gas region is constant and equal to zero. The liquid pressure right under the surface is related to the curvature of the surface by:

$$\frac{\sigma \dfrac{d^2\hat{\eta}}{d\hat{x}^2}}{\left(1 + \left(\dfrac{d\hat{\eta}}{d\hat{x}}\right)^2\right)^{3/2}} = - \hat{p}_\ell\ (\hat{x}, \hat{\eta}(\hat{x})) \tag{7}$$

Bernoulli's equation for the liquid pressure gives

$$- \hat{p}_\ell\ (\hat{x}, \hat{\eta}(\hat{x})) = + \frac{1}{2} \rho_\ell \left[\hat{u}^2(\hat{x}, \hat{\eta}(\hat{x})) + \hat{v}^2(\hat{x}, \hat{\eta}(\hat{x}))\right] + \rho_\ell\, g \hat{\eta}(x) \tag{8}$$

Far from the jet, we impose the boundary conditions:

$$\hat{\psi}\ (\hat{x} \to \infty, \hat{y}) = 0 \tag{9a}$$

$$\hat{\psi}\ (\hat{x}, \hat{y} \to \infty) = 0 \tag{9b}$$

We may make Eqs. (1)-(9) nondimensional, using x_o as the length scale and, V_ℓ as the velocity scale, respectively. Thus we have:

$$\nabla^2\psi = 0 \tag{10}$$

with boundary conditions,

$$\frac{\partial\psi}{\partial y}(x = 0, y) = 0 \tag{11a}$$

$$\psi\,(x, y\to\infty) = 0 \tag{11b}$$

$$\psi\,(x\to\infty, y) = 0 \tag{11c}$$

$$\frac{\partial\psi}{\partial x}(x, y=0) = +1 \qquad 0 < x < 1 \tag{11d}$$

$$\psi(x, \eta\,(x)) = 0 \qquad 1 < x \tag{11e}$$

where,

$$x = \hat{x}/x_o \quad , \quad y = \hat{y}/x_o \quad , \quad \eta = \hat{\eta}/x_o$$

$$u = \hat{u}/V_\ell \quad , \quad v = \hat{v}/V_\ell \quad \text{and} \quad \psi = \frac{\hat{\psi}}{x_o V_\ell}$$

The velocity components may now be computed from the stream function using Eqs. (2) and (3) as,

$$u(x,y) = \frac{\partial\psi}{\partial y}(x,y) \tag{12}$$

$$v(x,y) = -\frac{\partial\psi}{\partial x}(x,y) \tag{13}$$

The interfacial jump condition becomes

$$\frac{d^2\eta/dx^2}{\left(1+\left(\frac{d\eta}{dx}\right)^2\right)^{3/2}} = \left(\frac{1}{2}\rho_\ell \frac{V_\ell^2 x_o}{\sigma}\right)\left[u^2(x,\eta(x)) + v^2(x,\eta(x))\right] + \rho_\ell \frac{g\, x_o}{\sigma}\eta \tag{14}$$

Notice that the two multidimensional parameters are the Weber number, $We = \frac{1}{2}\rho_\ell \frac{V_\ell^2 x_o}{\sigma}$, and the Bond number, $B_o = \frac{\rho_\ell g\, x_o}{\sigma}$, which appear in the boundary condition, Eq. (14),

In order to solve the problem analytically we would have to obtain a solution of Laplace's equation, Eq. (10), that satisfies the boundary conditions, Eq. (11), where the free surface depression, $\eta(x)$, comes from Eq. (14). We note that the solution of Eq. (14) is linked to the solution of ψ through u and v; thus the problem is nonlinear.

We shall solve the problem for small We using a perturbation analysis. First, we may expand all the dependent variables in terms of We obtaining:

$$\eta(x) = \sum_{i=1}^{n} We^i \eta_i(x) + O(We^{n+1}) \tag{15a}$$

$$\psi(x,y) = \sum_{i=0}^{n} We^i \psi_i(x,y) + O(We^{n+1}) \tag{15b}$$

Next we substitute Eq. (15b) into Eq. (10) to obtain,

$$\nabla^2\psi = \nabla^2\psi_o + We\nabla^2\psi_1 + We^2\nabla^2\psi_2 + \ldots = 0 \tag{16}$$

Equation (16) holds for all We, and thus all ψ_i must independently satisfy Laplace equations:

$$\nabla^2\psi_o = 0 \tag{17a}$$

$$\nabla^2\psi_1 = 0 \tag{17b}$$

$$\nabla^2\psi_2 = 0 \tag{17c}$$

Using the same reasoning, it is easy to show that all the homogeneous boundary conditions, Eqs. (11a) - (11c), lead to:

$$\frac{\partial\psi_i}{\partial y}(x=0,y) = 0 \qquad (i \geq 0) \tag{18}$$

$$\psi_i(x,y\rightarrow\infty) = 0 \qquad (i \geq 0) \tag{19}$$

$$\psi_i(x\rightarrow\infty,y) = 0 \qquad (i \geq 0) \tag{20}$$

Let us next expand the boundary condition in Eq. (11d):

$$\frac{\partial\psi_o}{\partial x}(x,y=0) + We\frac{\partial\psi_1}{\partial x}(x,y=0) + We^2\frac{\partial\psi_2}{\partial x}(x,y=0) + \ldots = +1 \tag{21}$$

Obviously the zeroth order term must be equal to +1 and all other terms must be zero. Thus,

$$\frac{\partial\psi_o}{\partial x}(x,y=0) = +1 \tag{22}$$

and

$$\frac{\partial\psi_i}{\partial x}(x,y=0) = 0 \qquad i \geq 1 \tag{23}$$

The boundary condition in Eq. (11e), and the interfacial jump condition, Eq. (14), require special attention. Using Eq. (15b), Eq. (11e) can be rewritten as:

$$0 = \psi(x,\eta\,(x)) = \psi_o\,(x,\eta(x)) + We\,\psi_1(x,\eta(x)) + We^2\psi_2(x,\eta(x)) + \ldots \tag{24}$$

Performing an expansion of ψ_i in terms of We in the neighborhood of $\eta = 0$, we obtain:

$$0 = \psi_o(x,0) + \frac{\partial \psi_o}{\partial y}(x,0)\,\eta(x) + \frac{1}{2}\frac{\partial^2 \psi_o}{\partial y^2}(x,0)\,\eta^2(x) + \ldots$$

$$+ We\left[\psi_1(x,0) + \frac{\partial \psi_1}{\partial y}(x,0)\,\eta(x) + \frac{1}{2}\frac{\partial^2 \psi_1}{\partial y^2}(x,0)\,\eta^2(x) + \ldots\right] + \ldots \tag{25}$$

Substituting Eqs. (15a) and (12) into Eq. (25), and rearranging (ie, collecting terms of order We^i), we obtain:

$$0 = \psi_o(x,0) + \left[u_o(x,0)\,\eta_1(x) + \psi_1(x,0)\right] We$$

$$+ We^2\left(u_1\eta_1 + u_o\eta_2 + \frac{1}{2}\frac{\partial u_o}{\partial y}\eta_1^2 + \psi_2(x,0)\right) + O(We^3)$$

$$+ We^3\left(u_1\eta_2 + \frac{1}{2}\frac{\partial u_1}{\partial y}\eta_1^2 + u_2\eta_1 + u_o\eta_3 + \frac{\partial u_o}{\partial y}\eta_1\eta_2 + \frac{1}{6}\eta_1^3 + \psi_3(x,0)\right)$$

$$+ O(We^4) \ldots \tag{26}$$

Thus, the boundary conditions for $x > 1$ are,

$$\psi_o(x,0) = 0 \tag{27a}$$

$$\psi_1(x,0) = -\,u_o\eta_1 \tag{27b}$$

$$\psi_2(x,0) = -\left(u_1\eta_1 + u_o\eta_2 + \frac{1}{2}\frac{\partial u_o}{\partial y}\eta_1^2\right) \tag{27c}$$

$$\psi_3(x,0) = -\left(u_o\eta_3 + u_1\eta_2 + u_2\eta_1 + \frac{1}{2}\frac{\partial u_1}{\partial y}\eta_1^2 + \frac{\partial u_o}{\partial y}\eta_1\eta_2 + \frac{1}{6}\frac{\partial^2 u_o}{\partial y^2}\eta_1^3\right) \tag{27d}$$

Notice that ψ_i has homogeneous boundary conditions for $i \geq 1$, except for $x \geq 1$, where its value is given by Eqs. (27). This set of equations is the result of the asymptotic expansion of Eq. (11e). In order to obtain a closed set of equations, let us focus our attention on Eq. (14), the interfacial jump condition. We first expand the left hand side of Eq. (14) and then the right hand side.

The left hand side of Eq. (14) can be expanded as:

$$\frac{d^2\eta/dx^2}{\left(1+\left(\frac{d\eta}{dx}\right)^2\right)^{3/2}} = \frac{\frac{d^2}{dx^2}\left(\sum_{i=0}^{n} \eta_i(x)\, We^i + O(We^{n+1})\right)}{\left\{1+\left[\frac{d}{dx}\left(\sum_{i=0}^{n} \eta_i(x)\, We^i + O(We^{n+1})\right)\right]^2\right\}^{3/2}}$$

$$= \frac{d^2\eta_o}{dx^2} + \frac{d^2\eta_1}{dx^2}\,We + \frac{d^2\eta_2}{dx^2}\,We^2 + We^3\left(-\frac{3}{2}\frac{d^2\eta_1}{dx^2}\left(\frac{d\eta_1}{dx}\right)^2 + \frac{d^2\eta_3}{dx^2}\right)$$

$$+ We^4\left(-3\frac{d^2\eta_1}{dx^2}\frac{d\eta_1}{dx}\frac{d\eta_2}{dx} - \frac{3}{2}\frac{d^2\eta_2}{dx^2}\left(\frac{d\eta_1}{dx}\right)^2 + \frac{d^2\eta_4}{dx^2}\right) + O(We^5) \qquad (28)$$

Similarly, the right hand side of Eq. (14) can be expanded as,

$$We\left[u^2(x,\eta(x)) + v^2(x,\eta(x))\right] =$$

$$We\left\{\left[u_o(x,0) + \frac{\partial u_o}{\partial y}(x,0)\,\eta(x) + \frac{1}{2}\frac{\partial^2 u_o}{\partial y^2}(x,0)\,\eta^2(x) + \ldots\right.\right.$$

$$\left.+We\left(u_1(x,0) + \frac{\partial u_i}{\partial y}(x,0)\,\eta(x) + \frac{1}{2}\frac{\partial^2 u_1}{\partial y^2}(x,0)\,\eta^2(x) + \ldots\right)\right]^2$$

$$+\left[v_o(x,0) + \frac{\partial v_o}{\partial y}(x,0)\,\eta(x) + \frac{1}{2}\frac{\partial v_o}{\partial x^2}(x,0)\,\eta^2(x) + \ldots\right.$$

$$+ We\left(v_1(x,0) \quad \frac{\partial v_1}{\partial y}(x,0)\,\eta(x) + \frac{1}{2}\frac{\partial^2 v_1}{\partial y^2}(x,0)\,\eta^2(x) + \ldots \right)\Bigg]^2\Bigg\} \tag{29}$$

Using Eq. (15a) we obtain:

$$We\left[u^2(x,\eta(x)) + v^2(x,\eta(x))\right]$$

$$= We\left\{\left[u_o(x,0) + \frac{\partial u_o}{\partial y}(x,0)\,(\eta_o + We\,\eta_1 + We^2\eta_2 + \ldots) \quad + \ldots \right.\right.$$

$$\left. + We\left(u_1(x,0) + \frac{\partial u_1}{\partial y}(x,0)\,(\eta_o + We\,\eta_1 + We^2\eta_2 + \ldots)\right)\right]^2$$

$$+ \left[v_o(x,0) + \frac{\partial v_o}{\partial y}(x,0)\left(\eta_o(x) + We\,\eta_1 + We^2\eta_2 + \ldots\right) + \ldots \right.$$

$$\left.\left. + We\left(v_1(x,0) + \frac{\partial v_1}{\partial y}(x,0)\left(\eta_o + We\,\eta_1 + We^2\eta_2 + \ldots\right) + \ldots\right) + \ldots\right]^2\right\} \tag{29b}$$

Finally,

$$(u^2 + v^2)\,We = (u_o^2 + v_o^2)\,We + We^2\left(2u_o\left(\frac{\partial u_o}{\partial y}\eta_1 + u_1\right) + 2v_o\left(\frac{\partial v_o}{\partial y}v_1 + v_1\right)\right)$$

$$+ We^4\left\{2\left[\frac{\partial v_o}{\partial y}\eta_1 + v_1\right]\left[\frac{\partial v_1}{\partial y}\eta_1 + \frac{\partial v_o}{\partial y}\eta_2 + \frac{1}{2}\frac{\partial^2 v_o}{\partial y^2}\eta_1^2 + v^2\right]\right.$$

$$+ 2v_o\left[\frac{\partial v_1}{\partial y}\eta_2 + \frac{1}{2}\frac{\partial^2 v_1}{\partial y^2}\eta_1^2 + \frac{\partial v_2}{\partial y}\eta_1 + \frac{\partial v_o}{\partial y}\eta_3 + \frac{\partial^2 v_o}{\partial y^2}\eta_1\eta_2 + \frac{1}{6}\frac{\partial^3 v_o}{\partial y}\eta_1^3 + v_3\right]$$

$$\left. + 2u_o\left[\frac{\partial u_1}{\partial y}\eta_2 + \frac{1}{2}\frac{\partial^2 u_1}{\partial y^2}\eta_1^2 + \frac{\partial u_2}{\partial y}\eta_1 + \frac{\partial u_o}{\partial y}\eta_3 + \frac{\partial^2 u_o}{\partial y^2}\eta_1\eta_2 + \frac{1}{6}\frac{\partial^3 u_0}{\partial y^3}\eta_1^3 + u_3\right]\right.$$

$$+ 2\left[\frac{\partial u_o}{\partial y}\eta_1 + u_1\right]\left[\frac{\partial u_1}{\partial y}\eta_1 + \frac{\partial u_o}{\partial y}\eta_2 + \frac{1}{2}\frac{\partial^2 u_o}{\partial y^2}\eta_1^2 + u_2\right]\Bigg\} + \ldots \tag{30a}$$

Comparing the expression for the right hand side of Eq. (28) with the right hand side of Eq. (30a) we obtain:

$$\frac{d^2\eta_o}{dx^2} = B_o\,\eta_o \tag{31a}$$

$$\frac{d^2\eta_1}{dx^2} = +\,(u_o^2 + v_o^2) + B_o\,\eta_1 \tag{31b}$$

$$\frac{d^2\eta_2}{dx^2} = +\left(2\,u_o\left(\frac{\partial u_o}{\partial y}\eta_1 + u_1\right) + 2\,v_o\left(\frac{\partial v_o}{\partial y}\eta_1 + v_1\right)\right) + B_o\,\eta_2 \tag{31c}$$

The boundary conditions for these ordinary differential equations are:

$$\eta_i\,(x\to\infty) = 0 \tag{32a}$$

$$\frac{d\eta_i}{dx}\,(x\to\infty) = 0 \tag{32b}$$

Equations (27) and (31) are the expanded forms of Eqs. (11e) and (14), respectively. Equations (17), (18), (19), (20), (22) and (23) complete the set of equations to be solved.

ORDER ZERO SOLUTION

In the previous section we have established an infinite set of coupled equations for $\eta_i(x)$. In this section we will solve the order zero equation analytically (i.e., for the functions η_o, ψ_o, u_o, v_o). The equation for η_o is Eq. (31a),

$$\frac{d^2\eta_o}{dx^2} = +\,B_o\,\eta_o$$

with the boundary conditions

$$\eta_o(x\to\infty) = 0 \tag{33a}$$

$$\frac{d\eta_o}{dx}(x\to\infty) = 0 \tag{33b}$$

The solution is

$$\eta_o(x) = 0 \tag{34}$$

The differential equation for ψ_o is Eq. (17a),

$$\nabla^2\psi_o = 0$$

and the corresponding boundary conditions, Eqs. (18), (19), (20), (22) and (23), are:

$$\psi_o(x\to\infty,y) = 0 \tag{35a}$$

$$\psi_o(x,y\to\infty) = 0 \tag{35b}$$

$$\frac{\partial\psi_o}{\partial y}(x=0,y) = 0 \tag{35c}$$

$$\frac{\partial\psi_o}{\partial x}(x,y=0) = +1 \qquad 0 < x < 1 \tag{35d}$$

$$\frac{\partial\psi_o}{\partial x}(x,y=0) = 0 \qquad x > 1 \tag{35e}$$

It is convenient to use complex variables to solve this two-dimensional problem. Let Φ be a nondimensional complex analytic function given by,

$$\Phi(z) = \phi(x,y) + i\,\psi(x,y) \tag{36}$$

where, $z = x + i\,y$, and ϕ, ψ are the real and imaginary parts of $\Phi(z)$, respectively. The function $\Phi(z)$ is the complex potential, ϕ is the velocity potential function and

ψ is the corresponding steam function. The velocity components of u, v are given by,

$$u = \frac{\partial \phi}{\partial x} = \frac{\partial \psi}{\partial z} \tag{37a}$$

$$u = \frac{\partial \phi}{\partial y} = -\frac{\partial \psi}{\partial x} \tag{37b}$$

and,

$$\frac{d\Phi}{dz} = u - i\,v \tag{38}$$

We recall the boundary conditions (35d&e),

$$\frac{\partial \psi_o}{\partial x}(x,0) = \begin{cases} -1 & 0 < x < 1 \\ 0 & x > 1 \end{cases} \tag{39}$$

A function of x and y that satisfies these boundary conditions is:

$$\frac{\partial \psi_o}{\partial x} = \frac{1}{\pi}\left[\text{atg}\left(\frac{x-1}{y}\right) - \text{atg}\left(\frac{x+1}{y}\right)\right] \tag{40}$$

This expression is the imaginary part of the following analytic function

$$\frac{d\Phi}{dz} = \frac{1}{\pi}\left[\log(z-1) - \log(z+1)\right] \tag{41}$$

We may use Eq. (38) to calculate the velocity components

$$u_o = \text{Re}(\Phi) = \frac{1}{\pi}\left(\log\left[y^2 + (x-1)^2\right] - \log\left[y^2 + (x+1)^2\right]\right) \tag{42}$$

$$v_o = -\,\text{Im}(\Phi) = \frac{1}{\pi}\left(\text{atg}\,\frac{(x+1)}{y} - \text{atg}\,\frac{(x-1)}{y}\right) \tag{43}$$

Table-I shows the velocity of the zeroth order solution as well as the derivatives needed for solving Eqs. (27) and (31). We now have the solution of the problem to order zero.

In order to solve the problem to order-n, we must:

(1) Compute u_o (x,y=0) and v_o(x,y=0) using Eqs. (42) and (43).

(2) Solve η_1(x) from (31b), (32a), (32b) with η_o(x,0), v_o(x,0) from Eqs. (42) and (43).

(3) Compute ψ_1(x,0) from Eq. (27b) for x > 1 using η_1(x), u_o(x,0), v_o(x,0).

(4) Solve $\nabla^2\psi_1 = 0$ using ψ_1(x,0) to obtain ψ_1(x,y).

(5) Compute $u_1(x,0) = \frac{\partial\psi_1}{\partial y}(x,0)$, $v_1(x,0) = -\frac{\partial\psi_1}{\partial x}(x,0)$.

(6) Evaluate $\frac{d^2\eta_2}{dx^2}$ using Eq. (31c).

(7) Compute ψ_2(x,0) from Eq. (27c) for x > 1, using η_1, η_2, u_o, v_o, u_1, v_1.

(8) Solve $\nabla^2\psi_2 = 0$ using ψ_2(x,0).

RESULTS

Figure-3 shows the analytical results for the zeroth velocities v_o,u_o as a function of the lateral position x for different axial positions y. We note that, as expected, the jet is spreading as we move downward. Moreover, the singular point at x = 1 in the lateral velocity is clearly visible in Fig-3(a).

The problem consideed so far is spatially unbounded (x- > ∞,y- > ∞). However, in order to perform the numerical integration of Eqs. (17) and Eqs. (31) we need finite boundaries. Thus, we have taken the integration domain for 0 < x < D, 0 < y < D. In the computations D was chosen large enough to have the velocities at

the boundaries reduced to 1% of the maximum value V_ℓ. The corresponding physical problem is a jet of width h impacting a pool of width 2D of the same liquid. For convenience the jet contact angle was $\pi/2$, and η is measured from the contact line position. That is,

$$\eta(x=D) = 0 \tag{44a}$$

$$\frac{d\eta}{dx}((x=D) = 0 \tag{44b}$$

What follows is a detailed description of Steps (1) - (8) from the previous section.

Step (1): From Eqs. (42) - (43) $u_o(x,y=0)$ must be,

$$u_o(x,y=0) = \frac{1}{\pi}\log\frac{(x-1)}{(x+1)} \tag{45}$$

and, $v_o(x,y=0) = 0$.

Step (2): Equation (31b) results in the following ordinary differential equation,

$$\eta_1'' - B_o\eta_1 = -(u_o^2 + v_o^2) = -\frac{1}{\pi^2}\log^2\frac{(x-1)}{(x+1)} \tag{46}$$

for the interval $1 < x < D$ with the boundary conditions,

$$\eta_1(x=D) = 0 \tag{47a}$$

$$\frac{d\eta_1}{dx}(x=D) = 0 \tag{47b}$$

Equation (46) has an integrable singular point at which x=1. We have numerically evaluated Eq, (46) using a Runge-Kutta (RK) algorithm with adaptive stepsize. Figure-4(a) shows η_1 as a function of x.

Since Eq. (46) has a singular point at x=1 we have performed an asymptotic analysis of x near x=1 to verify the numerical result. Let us consider the solution of Eq. (46) in the neighborhood of x=1. An asymptotic expansion of the right hand side of Eq. (46) yields,

$$-\frac{1}{\pi^2}\log^2\frac{(x-1)}{(x+1)} \sim -\frac{1}{\pi^2}\log^2\frac{(x-1)}{2} \tag{48}$$

The solution which is valid asymptotically close to x=1 is,

$$\eta_1(x) = C_1 e^{\sqrt{B_o}\,x} + C_2 e^{-\sqrt{B_o}\,x}$$

$$+ e^{\sqrt{B_o}\,x}\int_1^x \log^2\left(\frac{t-1}{2}\right)e^{-\sqrt{B_o}\,t}\,dt$$

$$+ e^{-\sqrt{B_o}\,x}\int_1^x \log^2\left(\frac{t-1}{2}\right)e^{\sqrt{B_o}\,t}\,dt \tag{49}$$

The main contribution for the integrals on the right hand side of Eq. (49) comes from small values of (t-1). Thus we can expand the exponentials as,

$$e^{\pm\sqrt{B_o}\,t} = e^{\pm\sqrt{B_o}}\,e^{\pm\sqrt{B_o}\,(t-1)} = e^{\pm\sqrt{B_o}}\left(1 \pm \sqrt{B_o}\,(t-1) + \sigma\left((t-1)^2\right)\right) \tag{50}$$

With this analysis we have shown that the singularity at x=1 is an integrable one. Tne results of the asymptotic expansion are shown in Fig. 4 as a line which essentially coincides with the numerical result. Indeed, the difference between the RK solver and the asymptotic expansion result is smaller than $10^{-4}\%$.

Step (3): $\psi_1(x,y=0)$ is computed using Eq. (27b).

$$\psi_1(x,y=0) = -\,u_o(x,y=0)\,\eta_1(x) \tag{51}$$

The resulting boundary condition for ψ_1 is shown in Fig. 5(a). Notice that ψ_1 has a singularity in x=1 due to u_o.

Step (4): The Laplace equation for ψ_1 has to be solved with the boundary conditions (BC) given in Eqs. (18)-(23). We numerically solved the Laplace equation using a five points finite difference scheme. A nine points scheme was also implemented into no noticeable improvement over the five point scheme. The velocities u_1, v_1 were computed using a differentiating centered first order. The region near x = 1 was highly refined because the boundary condition ψ_1 is singular there ($\sim \log \frac{(x-1)}{2}$).

We have verified the resulting ψ_1 using an asymptotic expansion of Eq. (52):

$$\psi_1(x,0) = - u_o \eta_1 \approx - \frac{n_1(x=1)}{\pi} \log(x-1) = \psi_1^{asym}(x,0) \qquad , (1 < x < D)$$

$$\psi_1(x,0) = 0 = \psi_1^{asym}(x,0) \qquad , (0 < x < 1) \tag{53}$$

An analytic continuation of Eq. (53) gives,

$$\psi_1^{asym}(z) = - \frac{\eta_1(x-1)}{\pi} \left[\frac{3}{4} \log (z-1) - \frac{i}{2\pi} \log [i(z-1)] \log(z-1) \right] \tag{54}$$

The real part of Eq. (54) is a solution of the Laplace equation and has the same asymptotic behavior at ψ_1 near x=1.

Notice that although $\psi_1(x,0) \approx \psi_1^{asym}(x,0)$, ψ_1 becomes significantly different than ψ_1^{asym} as we move away from the singularity, the results near x=1 are almost coincident. We have taken advantage of the linearity of the Laplace equation solving numerically for the difference between ψ_1 and ψ_1^{asym}. That is, we define

$$\psi_1^{diff}(x,y) = \psi_1(x,y) - \psi_1^{asym}(x,y) \tag{55}$$

Notice that $\psi_1^{diff}(x=1,y=0) = 0$ and therefore the singularity at x=1 has been removed. The boundary conditions for ψ_1^{diff} are:

$$\psi_1^{diff}(x,0) = \psi_1(x,0) - \psi_1^{asym}(x,0) \tag{56a}$$

$$\frac{\partial \psi_1^{diff}}{\partial x}(x,0) = 0 \tag{56b}$$

$$\psi_1^{diff}(x,y=0) = - \psi_1^{asym}(x,D) \tag{56c}$$

$$\psi_1^{diff}(x=D,y) = - \psi_1^{asym}(D,y) \tag{56d}$$

$$\psi_1^{diff}(x=0,y) = 0 \tag{56e}$$

$\psi_1(x,y)$ was numerically evaluated using the Laplacian solver with Eqs. (56). We note that these BCs have no singularities. Finally, the stream function and the velocities are computed using

$$\psi_1(x,y) = \psi_1^{diff}(x,y) + \psi_1^{asym}(x,y) \tag{57a}$$

$$u_1(x,y) = u_1^{diff}(x,y) + u_1^{asym}(x,y) \tag{57b}$$

$$v_1(x,y) = v_1^{diff}(x,y) + v_1^{asym}(x,y) \tag{57c}$$

The maximum difference between ψ_1, u_1, v_1 computed usign Eqs. (56) and (57), and by the Laplacian solver applied to Eq. (52), was less than 2% for the stream function and less than 5% for the velocities.

Step (5): u_1 and v_1 were computed from the stream function ψ_1. Figure 6 and 7 show both velocity iterates as a function of the position.

Step (6): We calculated η_2 from Eq. (31c) using the RK solver. We verified the solution in the neighborhood of x=1 as described previously. The result is shown in Fig. 4. We see that the x interval, where η_2 is significantly different than zero, is smaller than the range where η_1 was significantly different than zero. This is a general result of our calculations. The higher the order of the iterate, the smaller the range where the values of the iterate are significantly different from zero.

Step (7): We compute $\psi_2(x,0)$ using Eq. (31c). The result is shown in Fig. 5.

Step (8): We numerically solved for $\psi_2(x,0)$ using the Laplacian solver. We verified the numerical result as described for ψ_1. Notice that we had to keep track of three singularities in Eq. (27c). That is,

$$\psi_2(x,0) = -\left(u_1\eta_1 + x_o\eta_2 + \frac{1}{2}\frac{\partial x_o}{\partial y}\eta_1^2\right)$$

$$\sim -\eta_1(x=1)\, u_1^{asym}(x,0) - \eta_2(x=1)\, u_o^{asym}(x,0) + \frac{1}{2}\eta_1^2(x=1)\frac{\partial u_o^{asym}}{\partial y}(x,0)$$

$$= \psi_{21}^{asym} + \psi_{22}^{asym} + \psi_{23}^{asym} \tag{58}$$

then we obtained,

$$\psi_2^{asym}(z) = \psi_{22}^{asym}(z) + \psi_{22}^{asym}(z) + \psi_{23}^{asym}(z) \tag{59}$$

The stream functions $\psi_{21}, \psi_{22}, \psi_{23}$ were obtained with the help of a symbolic manipulator an because of their complexity the results will not be presented herein. As before, ψ_2^{diff} is defined as,

$$\psi_2^{diff} = \psi_2 - \psi_2^{asym} \tag{60}$$

The velocity iterates u_2 v_2 are shown in Figs. 6&7.

Step (9): The third order iterates η_3, ψ_3, u_3, v_3 were computed following a similar procedure. The results are shown in Figs. (4)-(7). We see that significant values of the third order iterates are restricted to a smaller range than the second order iterates.

Figure 8 shows the position of the interface η as a function of the lateral position x for values of the Weber number in the range [0.1 to 0.8]. We now analyze the behavior of the $\eta(x)$ as we move from the rightmost position in the plot (x=1.1) to lower values of x. For We = 0.01, $\eta(x)$ increases as x approaches the jet impact point x = 1 without any local minimum (ie, no surface depression is present). For We = 0.8, on the other hand, as x is decreased, we first have a local minimum in η, (η^{max}), and then a local minimum (η^{min}, depression is present). We define the depth of the depression, d, as:

$$d = \eta^{max} - \eta^{min} \tag{61}$$

Figure 9 shows the depth of the depression d as a function of the Weber number. There is no depression (d=0) up to a critical Weber number (We_c). For We larger than the critical value, the depth of the depression increases rapidly with the We.

The depression width δ is defined as the gas gap corresponding to a depression of d/2. Figure 10 shows the depression width δ as a function of the We number. We see that for high We numbers δ levels off to a value of about 0.013.

Finally, we present a set of results where the effect of gravity has been investigated. In Figs. 11-17 the Bond number is equal to Bo = 1. The interface position iterates, η_i(Bo = 1), have the same qualitative shape compared to η_i(Bo = 0). However, the magnitude of the iterates is larger in the case with Bo = 1. The same is true for the stream function and velocities iterates. This effect is a direct consequence of the larger values of the η_i. Notice that u_o has the same value in the

Bo = 0 and Bo= 1 calculations. Thus, if $|\eta_1(Bo = 1)|$ is greater than $|\eta_1(Bo = 0)|$ the same relationship will hold between $|\psi_1(Bo = 1)|$ and $|\psi_1(Bo = 0)|$.

Figure 15 shows the position of the interface as a function of the lateral position for different We number. The most noticeable effect of the gravity is to flatten the interface.

Figure 16 shows the depth of the depression (d) as a function of the We number for Bo = 1. The interface has a larger depression for Bo = 1 than Bo = 0. Figure 17 shows the width of the depression as a function of the We number for Bo = 1. Surprisingly, even though the shape of the interfaces are different than the Bo = 0 the width is nearly equal.

SUMMARY AND CONCLUSIONS

This paper presents the results of an analysis based on a nonsingular perturbative technique for the surface depression produced by a plunging liquid jet. The first three terms of a Taylor series expansion in the Weber number have been obtained for the surface depression. This approximation of the surface depression gives correct values for small and moderate Weber numbers (ie, We < 1). However, for We greater than unity, higher order terms become important and the analysis presented here is no longer valid. The Bond number appears as a parameter in the system of equations. No expansion is necessary for the Bond number. The analysis presented here is valid for all Bo numbers.

The results described in this paper show that as the Weber number is increased, the terms that gain importance (i.e., the terms of higher order) correspond to a surface depression that is increasingly narrower in the horizontal direction. For a Weber number of the order of unity the surface tension is no longer strong enough to keep the system stable and an instability leads to air entrainment. That is, for values of the surface tension going to infinity (i.e., Weber number going to zero),

the slope of the surface is very small, however, as the Weber number is increased the slope also increases. For a critical value of the Weber number, the slope of the surface is such that the surface tension is not large enough to keep the pool surface from getting near the plunging liquid jet and thus air entrainment is produced. We have assumed in this paper that the position of the interface can be written as $\eta(x)$, that is a steady state exists where the position of the interface is a single-valued function of the lateral position. For the critical value of the Weber number that corresponds to the threshold for air entrainment the interface is not a single-valued and also it is likely the air entrainment process involves a transient phenomena. Thus we believe that our analysis is not appropriate to compute the threshold value of the Weber number for air entrainment. However, we are able to describe the route to air entrainment qualitatevily. We have seen that the higher the order of the position of the interface iterate, the larger the maximum slope of the iterate. For small We numbers the low order iterates dominate. As the We number is increased, the slope of the interface is increased because higher order terms dominate. For a value of We the interface has a very large slope (tangent of the interface almost vertical). For a We>Wet the inertia forces overpower the capillary forces and the interface is not stable any more.

The results presented in this paper cannot predict the route to instability that produces air entrainment for two reasons. First, it is not clear that the approximation of the surface depression is valid for Weber numbers that are high enough to produce air entrainment. Second, the shape of the surface, $\eta(x)$, has to be a monovalued function of x and it appears that at the point where air entrainment is produced, for every x (horizontal position) there is more than one η (vertical position of the surface depression).

It appears that it would be useful to compute the surface position using an appropriate multidimensional Computational Fluid Dynamics (CFD) tool having surface tracking capability. This will allow the relaxation of the small and moderate Weber numbers assumption.

ACKNOWLEDGMENT

The financial support of this study by the Office of Naval Research (ONR) Grant No. N-0001491-J-1271 of the ONR Fluid Dynamics Program-1132F is gratefully acknowledged.

REFERENCES

Bonetto, F., Drew, D.A. and Lahey, R.T., Jr., "The Analysis of a Plunging Jet - The Air Entrainment Process," accepted for publication in *J. of Chemical Engineering Communications*, 1993.

Kerman, B.R., "A Model of Interfacial Gas Transfer for a Well-Roughened Sea," *J. of Geophysical Research*, Vol. 89 (D1), pp. 1439-1446, 1984.

Lezzi, A.M. and Prosperetti, A., "The Stability of an Air Film in a Liquid Flow," *J. Fluid Mech.*, Vol. 226, pp. 319-347, 1991.

Monahan, R. and Torgersen, T., in *Air-Water Mass Transfer*, ed. Wilhelms and Gulliver, pp. 608-617, 1991.

TABLE-I

SUMMARY OF THE ORDER-ZERO SOLUTIONS

$$u_o(x,0) = \frac{1}{\pi} \log \frac{x-1}{x+1}$$

$$v_o(x,0) = 0$$

$$\frac{\partial u_o}{\partial y}(x,0) = 0$$

$$\frac{\partial v_o}{\partial y}(x,0) = \frac{2}{\pi(x-1)(x+1)}$$

$$\frac{\partial^2 u_o}{\partial y^2}(x,0) = \frac{4x}{\pi(x-1)^2(x+1)^2}$$

$$\frac{\partial^2 v_o}{\partial y^2}(x,0) = 0$$

$$\frac{\partial^3 u_o}{\partial y^3}(x,0) = 0$$

$$\frac{\partial^3 v_o}{\partial y^3}(x,0) = -\frac{4(3x^2+1)}{\pi(x-1)^3(x+1)^3}$$

$$u_o(x,y) = \frac{1}{2\pi} \log \left(\frac{y^2 + (x-1)^2}{y^2 + (x+1)^2} \right)$$

$$v_o(x,y) = \frac{1}{\pi} \left(\text{atg} \frac{x+1}{y} - \text{atg} \frac{x-1}{y} \right)$$

FIGURE CAPTIONS

Figure 1 Illustration of the surface depression produced by a plunging liquid jet.

Figure 2 Boundary conditions for the stream function

$\hat{y} = \infty$ $\hat{\psi} = 0$ $\hat{\psi} = 0$

$\hat{x} = \infty$ $\hat{y}$ $\hat{x}$ x_o v_l v_l

symmetry plane

Figure 3(a) Solution of the transverse velocity of order zero for different axial positions: (a) y=0 (undisturbed pool surface level), (b) y=0.5, (c)y=1., and (d) y=2.

(a) (b) (c) (d) x

Figure 3(b) Solution of the axial velocity of order zero for different axial positions: (a) y=0 (undisturbed pool surface level), (b) y=0.5, (c)y=1., and (d) y=2.

(a) (b) (c) (d) x

Figure 4 Iterates of the surface position, $\eta_i(x)$, corresponding to Bo=0

η_1

η_2

η_3

x

Figure 5 Iterates of the surface stream function, $\psi_i(x,y=0)$, corresponding to Bo=0

ψ_1

ψ_2

ψ_3

x

Figure 6 Iterates of the lateral velocity, $u_i(x,y=0)$, corresponding to Bo=0

u_1

u_2

u_3

x

Figure 7 Iterates of the axial velocity, $v_i(x,y=0)$, corresponding to Bo=0

v_1

v_2

v_3

x

Figure 8 Shape of the interface for different Weber numbers(Bo=0)

η x We = 0.1 We = 0.8

Figure 9 Gas gap depth d as a function of the Weber number (Bo=0).

Figure 13 Definition of the gas gap width, δ

Liquid
Jet

Figure 10 Gas gap width δ as a function of the Weber number (Bo=0)

δ We

Figure 11 Iterates of the surface position, $\eta_i(x)$, corresponding to Bo=1

η_1

η_2

η_3

x

Figure 12 Iterates of the surface stream function, $\psi_i(x,y=0)$, corresponding to Bo=1

ψ_1

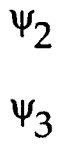

Figure 13 Iterates of the lateral velocity, $u_i(x,y=0)$, corresponding to Bo=1

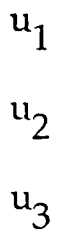

Figure 14 Iterates of the axial velocity, $v_i(x,y=0)$, corresponding to Bo=1

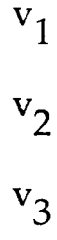

Figure 15 Shape of the interface for different Weber numbers(Bo=1)

Figure 16 Gas gap depth d as a function of the Weber number (Bo=1).

Figure 17 Gas gap width δ as a function of the Weber number (Bo=1)

δ We

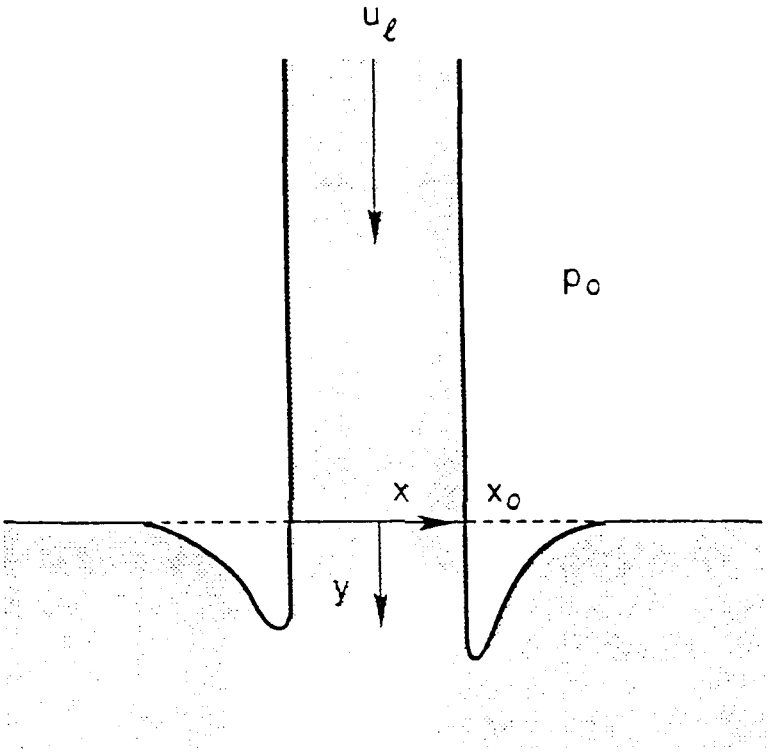

Figure 1 Illustration of the surface depression produced by a plunging liquid jet.

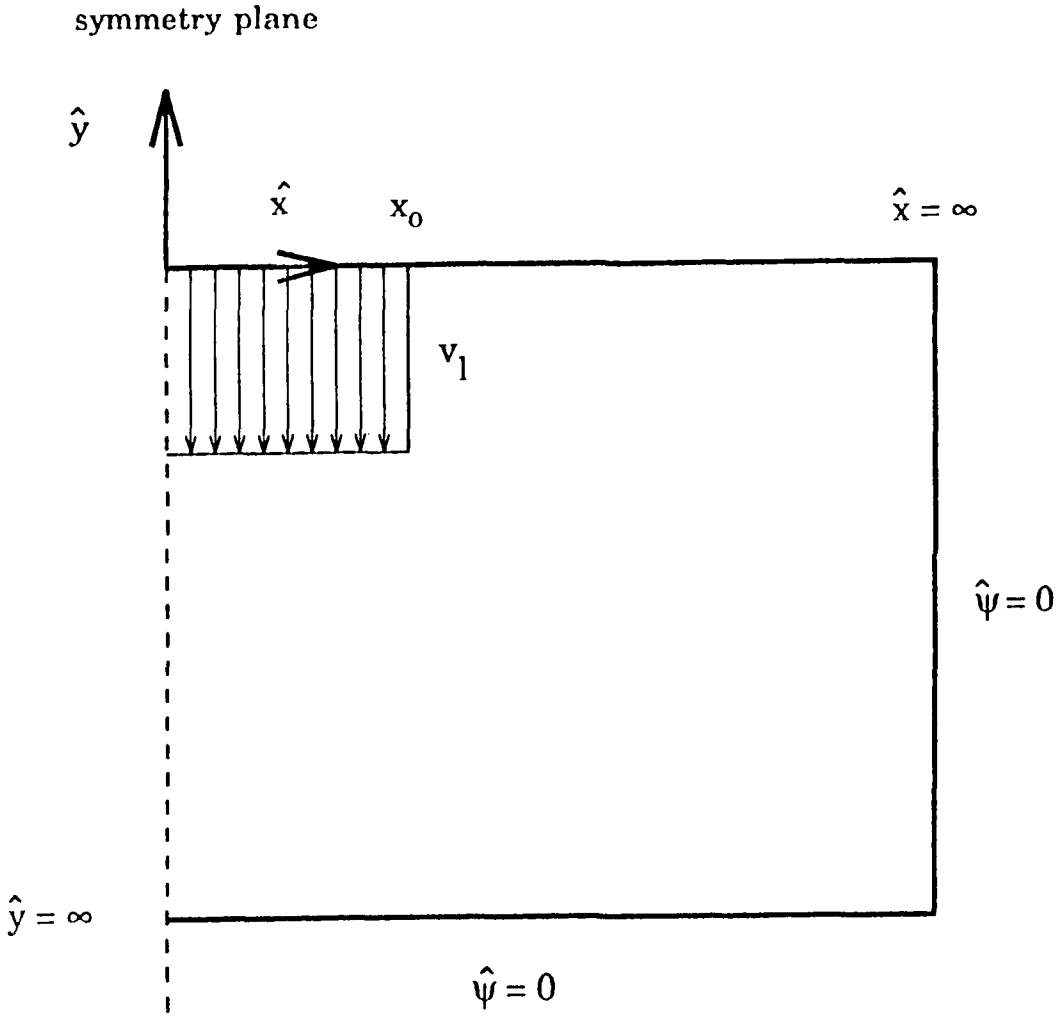

Figure 2 Boundary conditions for the stream function

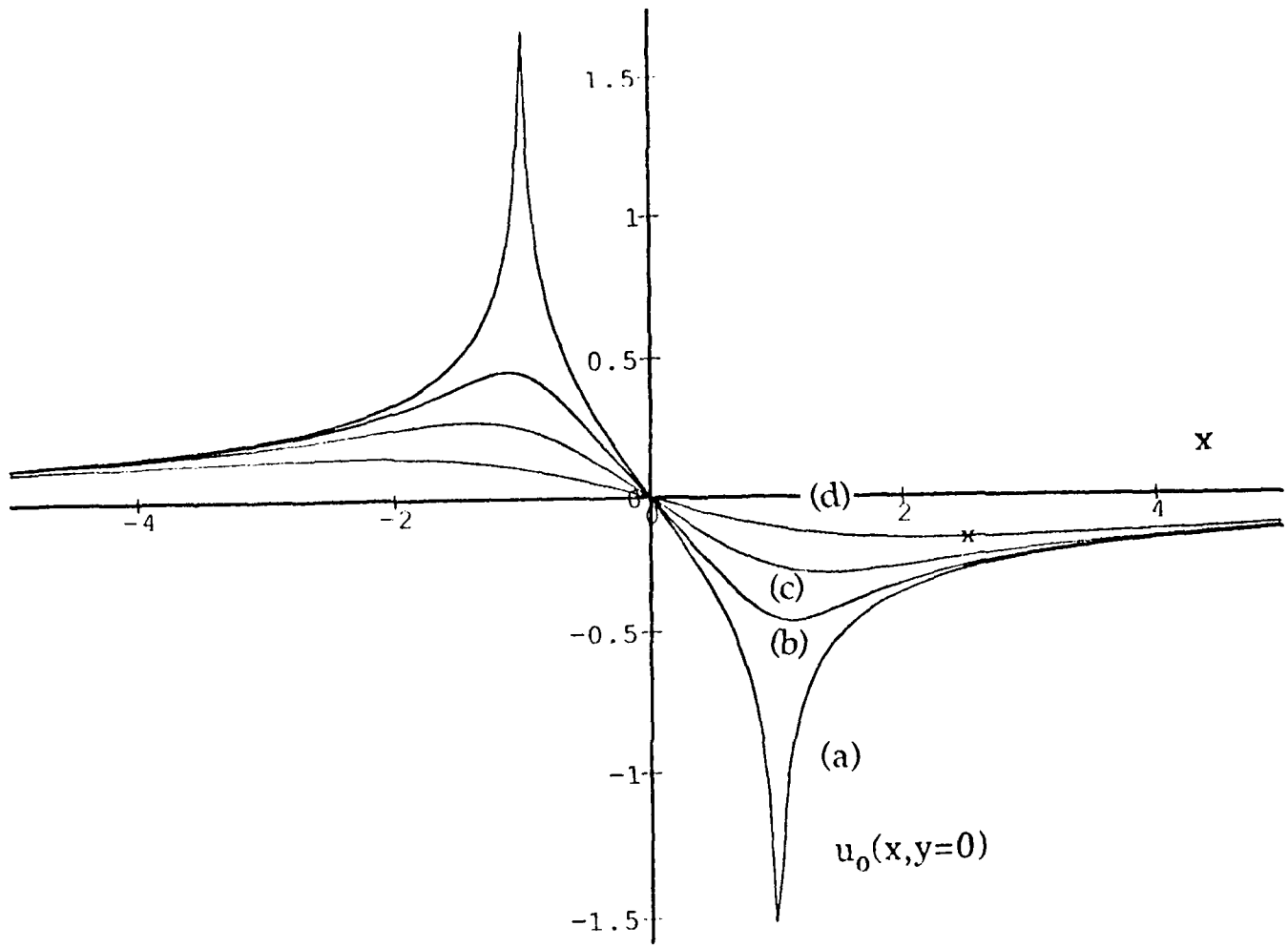

Figure 3(a) Solution of the transverse velocity of order zero for different axial positions: (a) y=0 (undisturbed pool surface level), (b) y=0.5, (c)y=1., and (d) y=2.

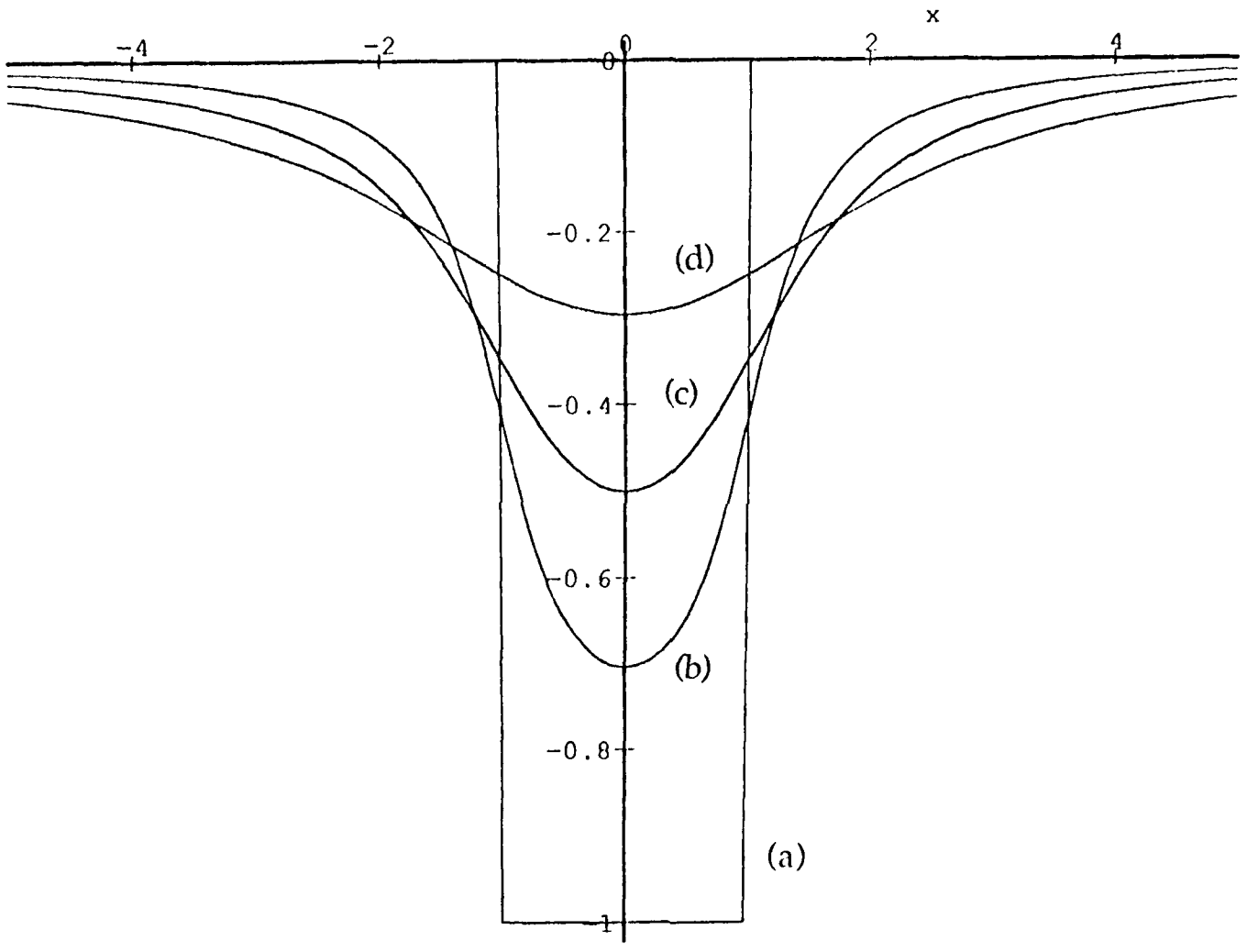

Figure 3(b) Solution of the axial velocity of order zero for different axial positions: (a) y=0 (undisturbed pool surface level), (b) y=0.5, (c)y=1., and (d) y=2.

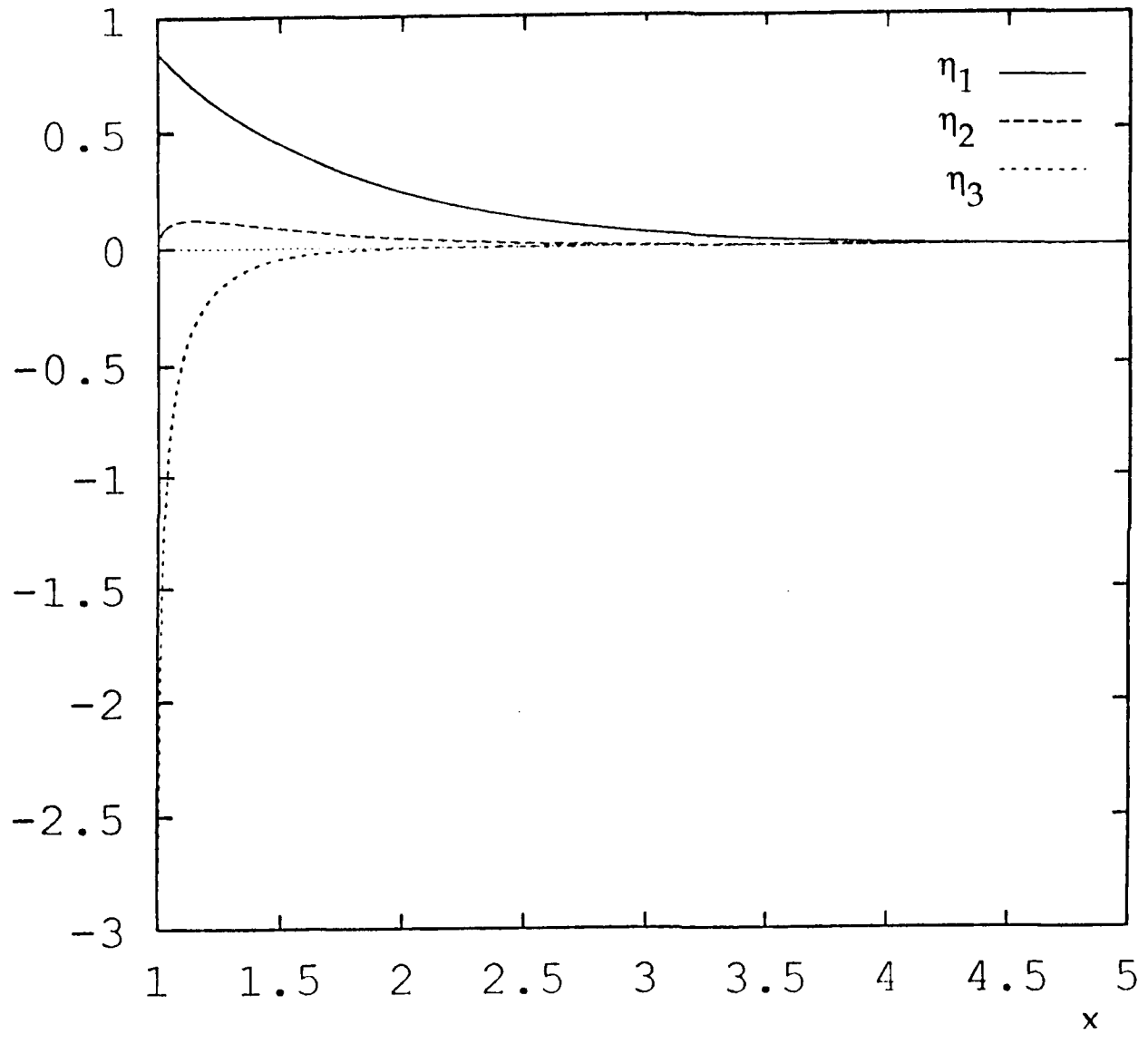

Figure 4 Iterates of the surface position, $\eta_i(x)$, corresponding to Bo=0

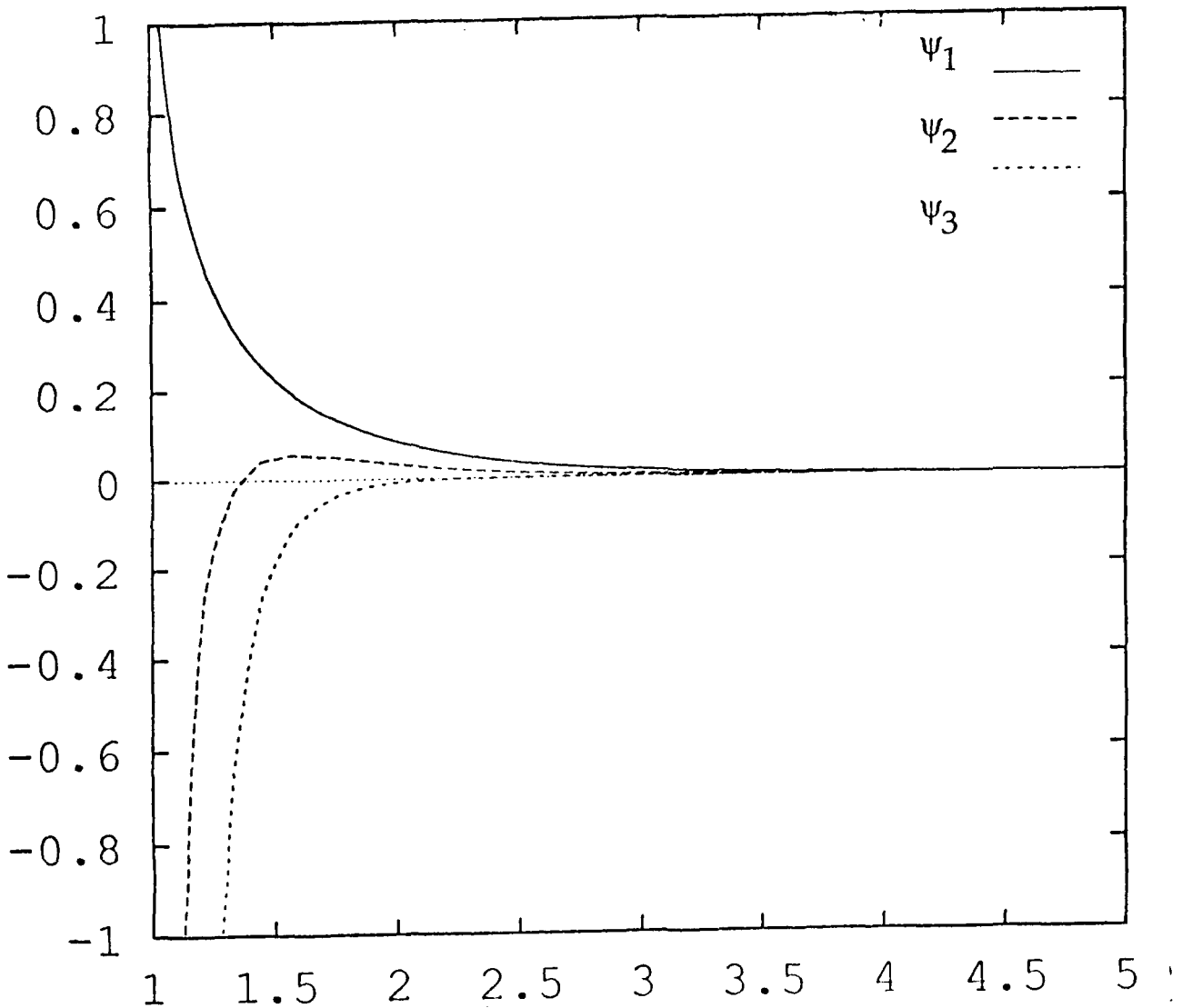

Figure 5 Iterates of the surface stream function, $\psi_i(x,y=0)$, corresponding to Bo=0

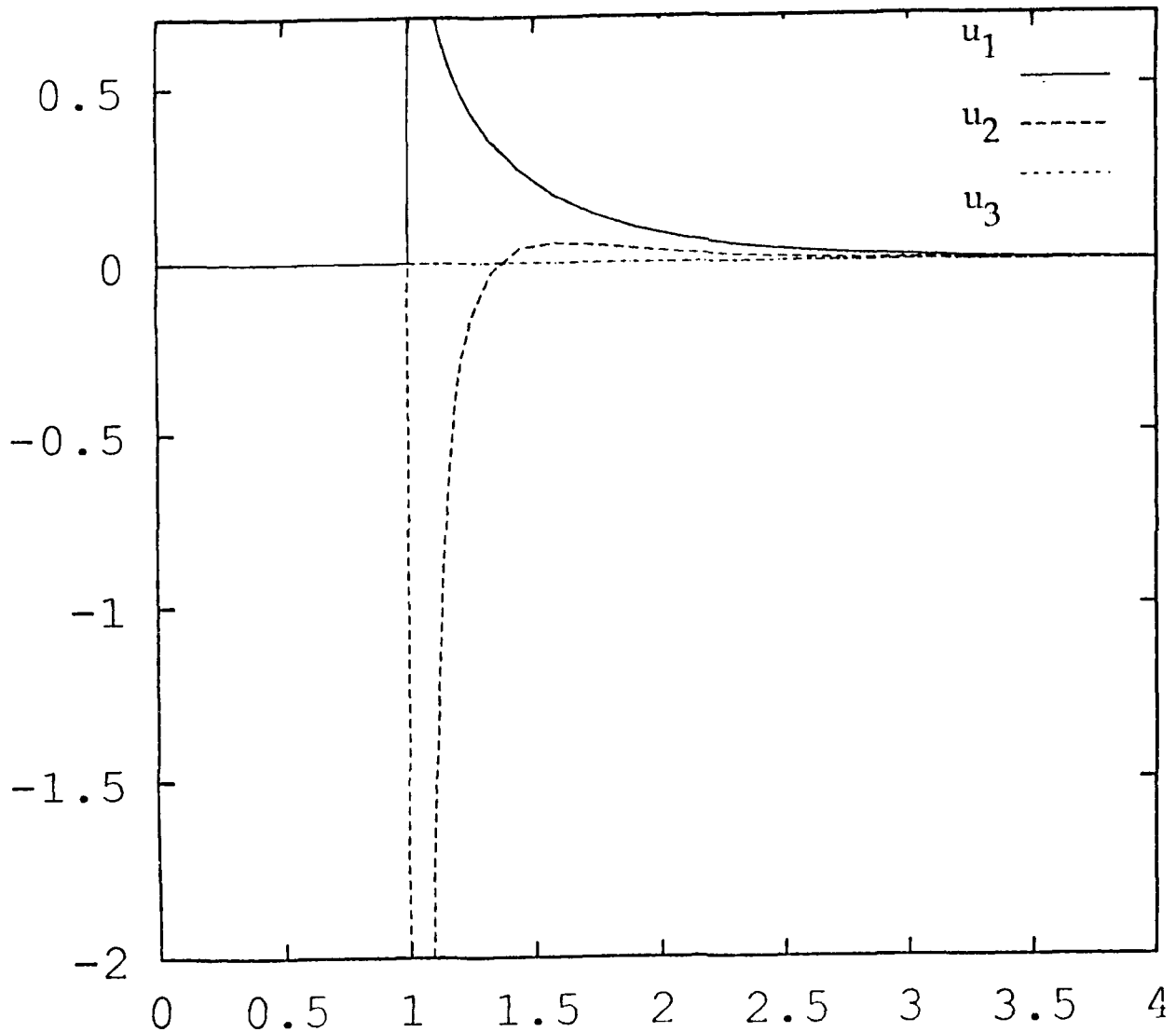

Figure 6 Iterates of the lateral velocity, $u_i(x,y=0)$, corresponding to Bo=0

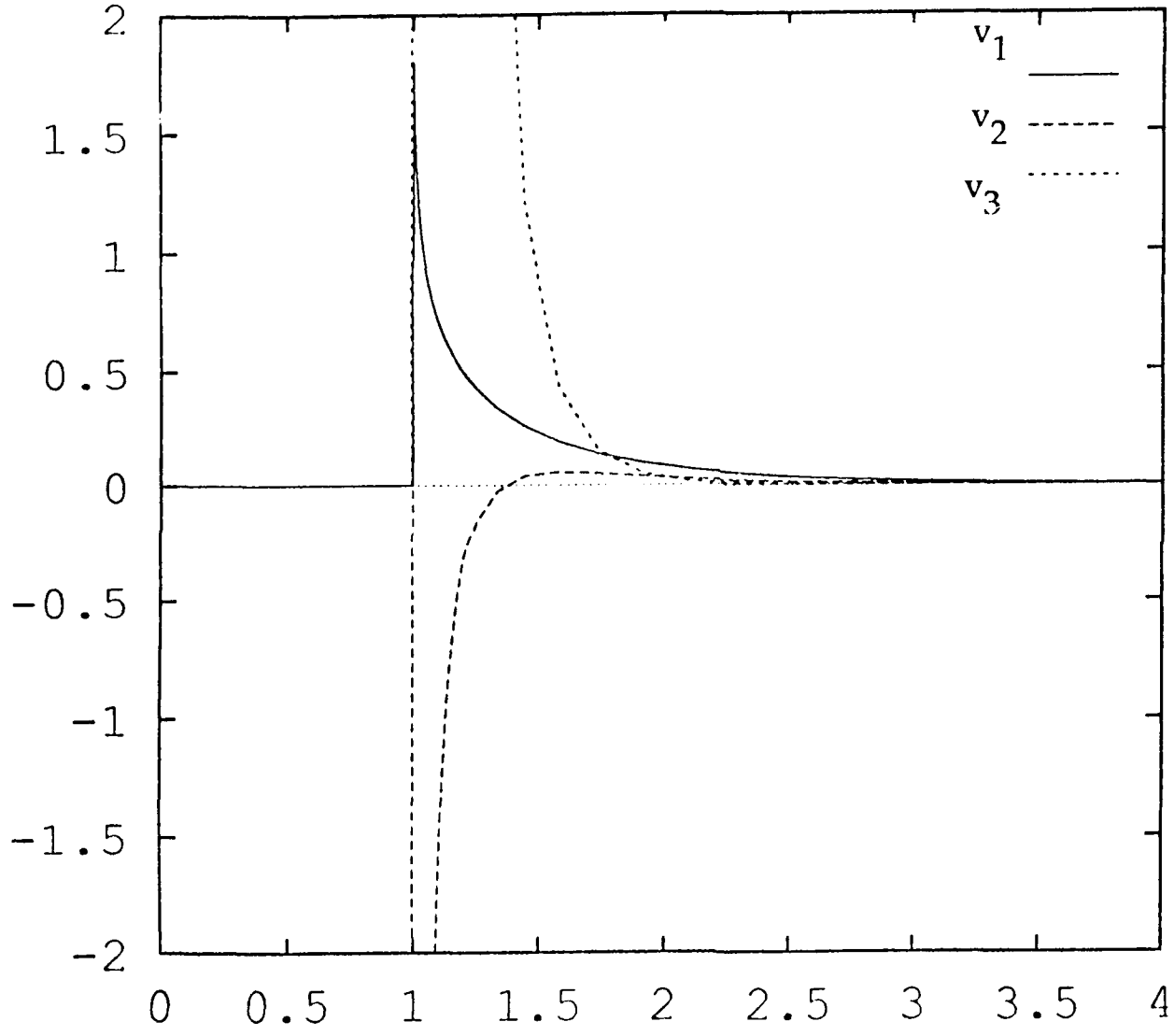

Figure 7 Iterates of the axial velocity, $v_i(x,y=0)$, corresponding to Bo=0

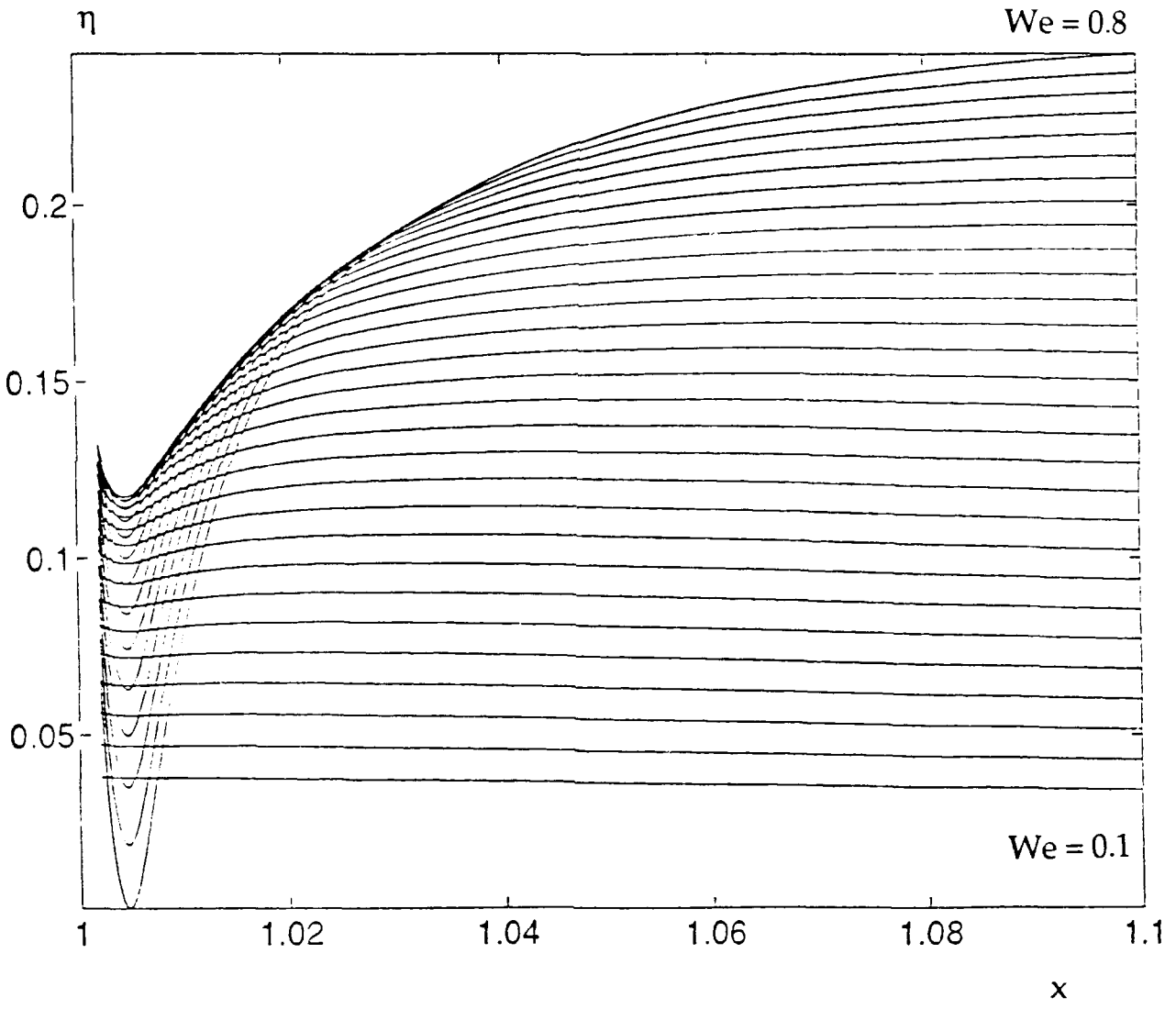

Figure 8 Shape of the interface for different Weber numbers(Bo=0)

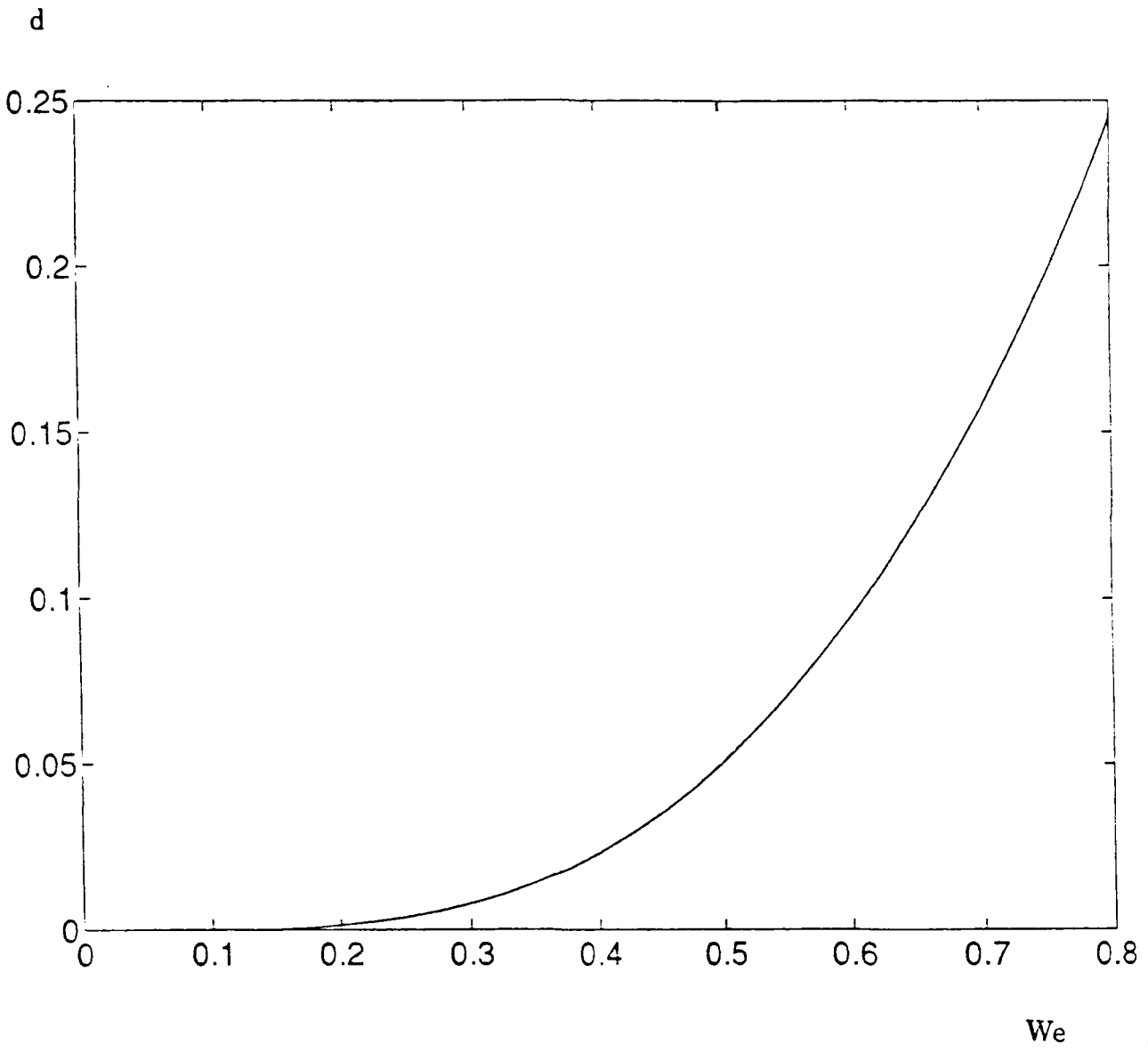

Figure 9 Gas gap depth d as a function of the Weber number (Bo=0).

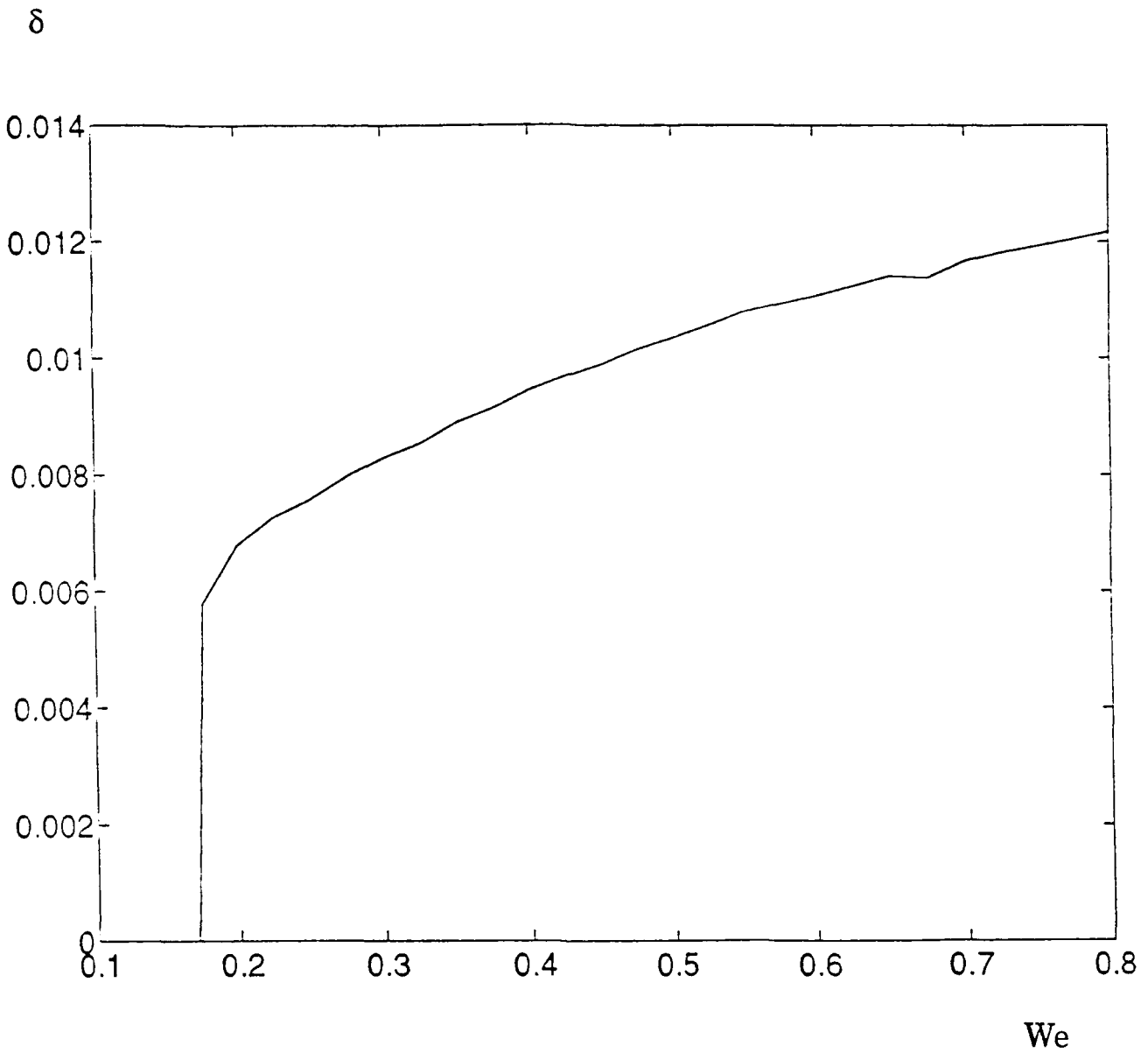

Figure 10 Gas gap width δ as a function of the Weber number (Bo=0)

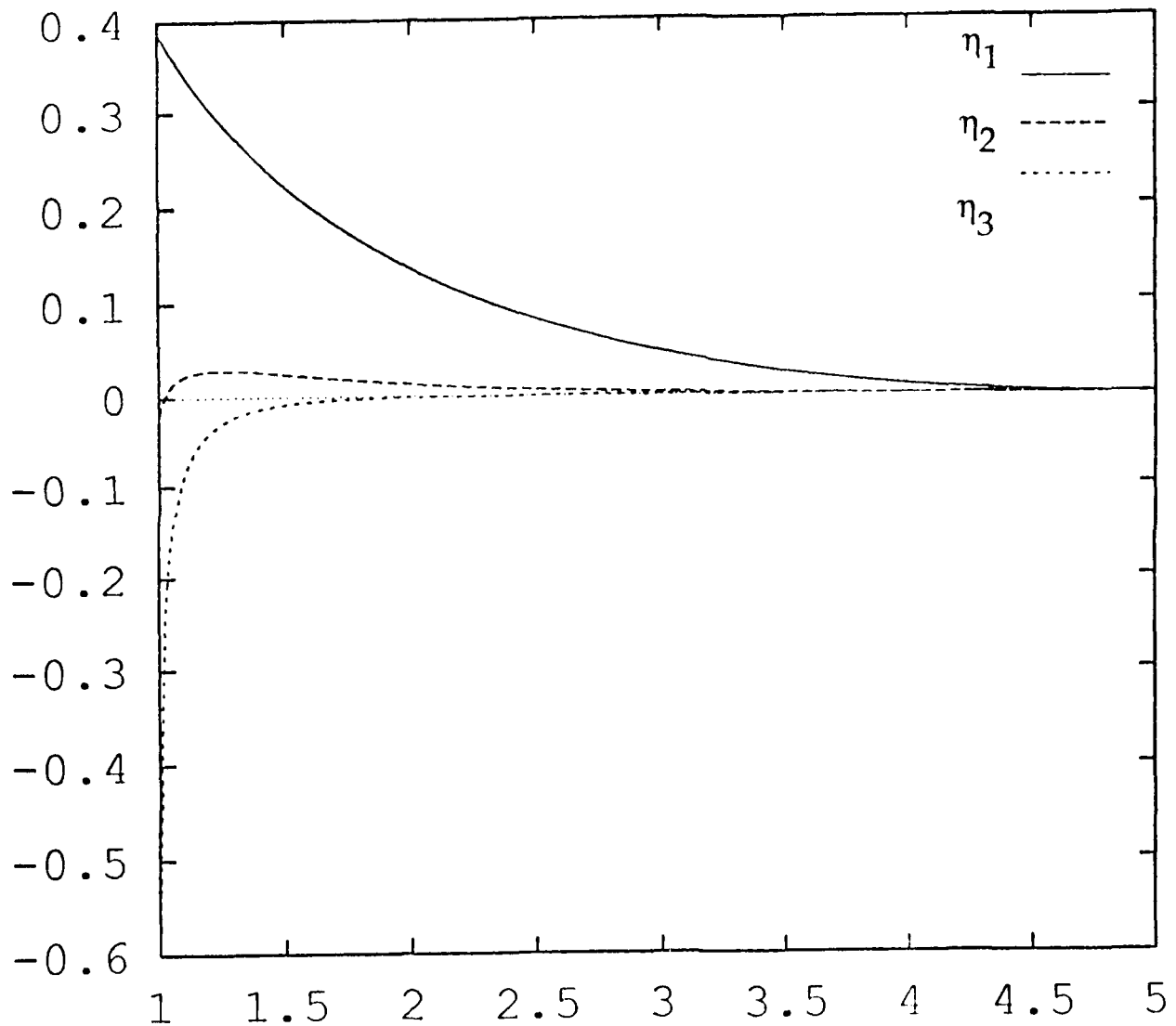

Figure 11 Iterates of the surface position, $\eta_i(x)$, corresponding to Bo=1

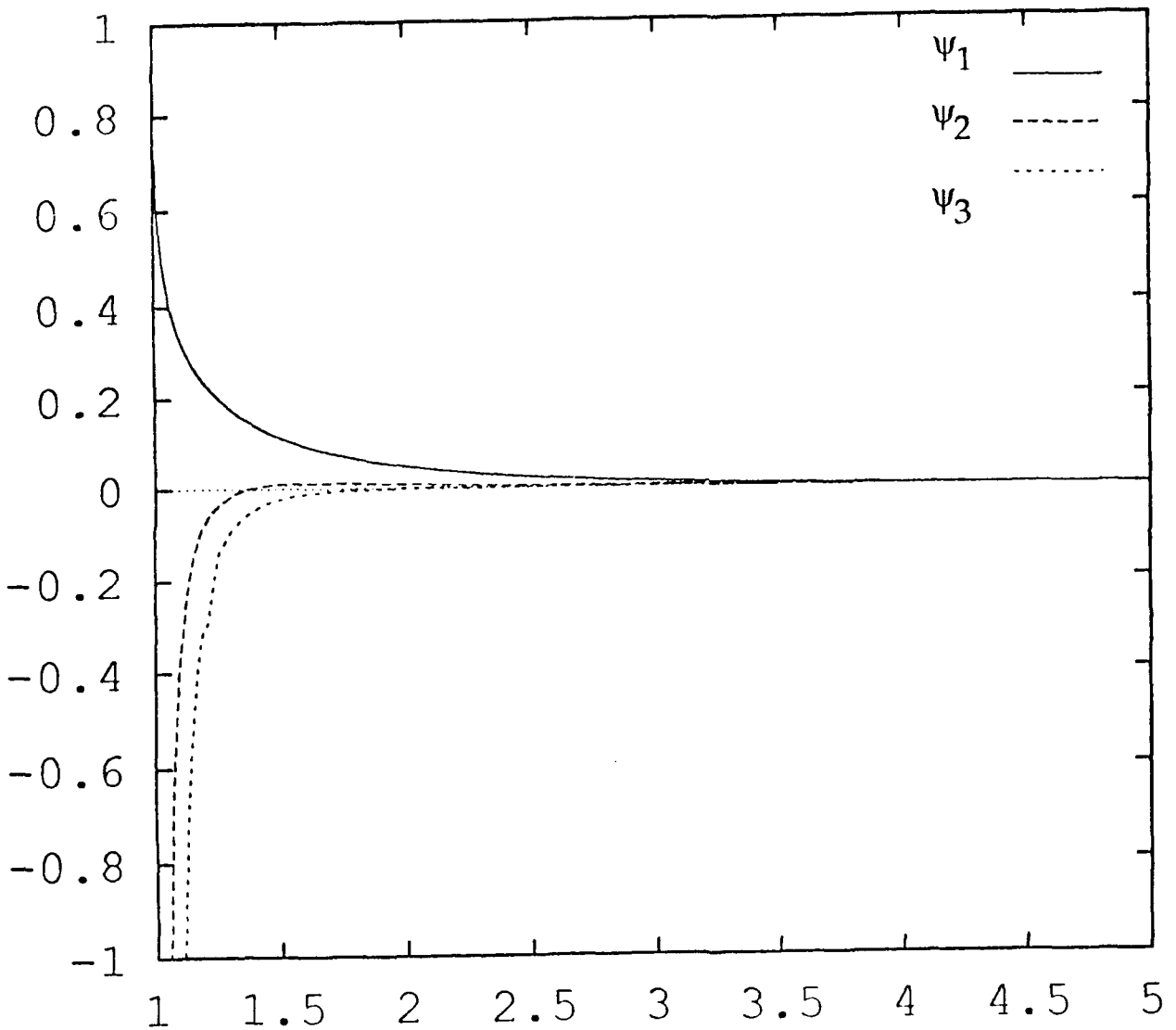

Figure 12 Iterates of the surface stream function, $\psi_i(x,y=0)$, corresponding to Bo=1

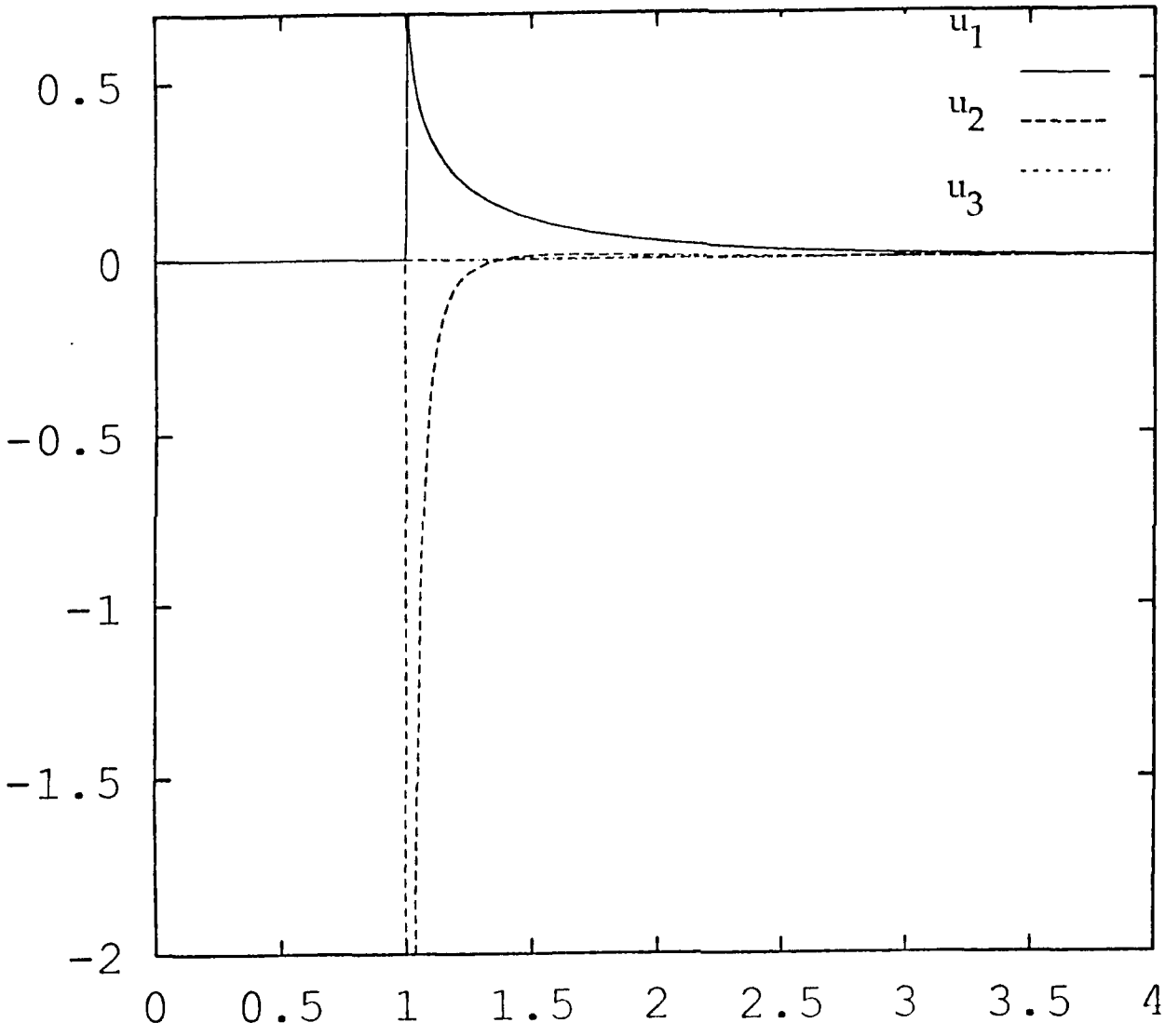

Figure 13 Iterates of the lateral velocity, $u_i(x,y=0)$, corresponding to Bo=1

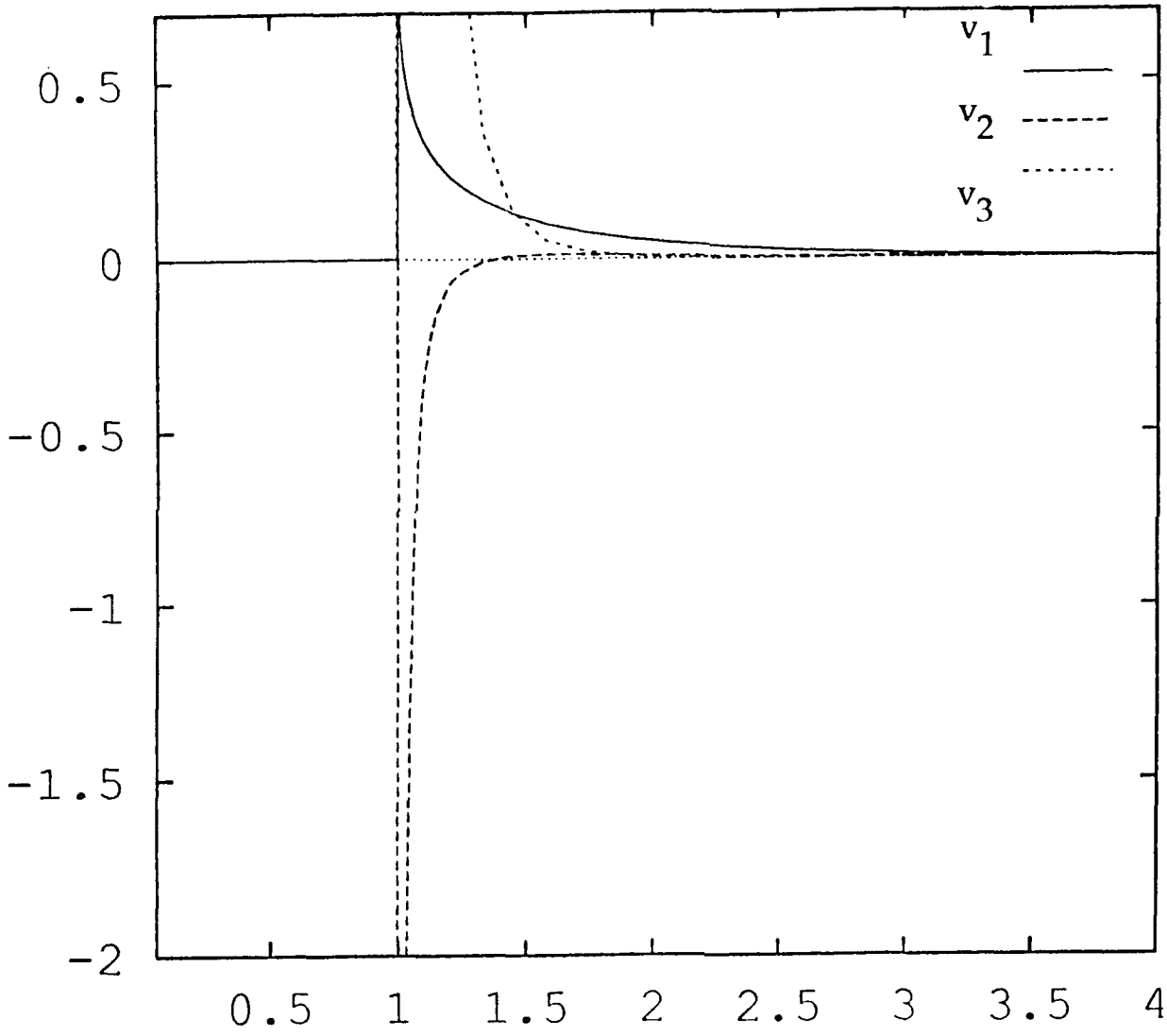

Figure 14 Iterates of the axial velocity, $v_i(x,y=0)$, corresponding to Bo=1

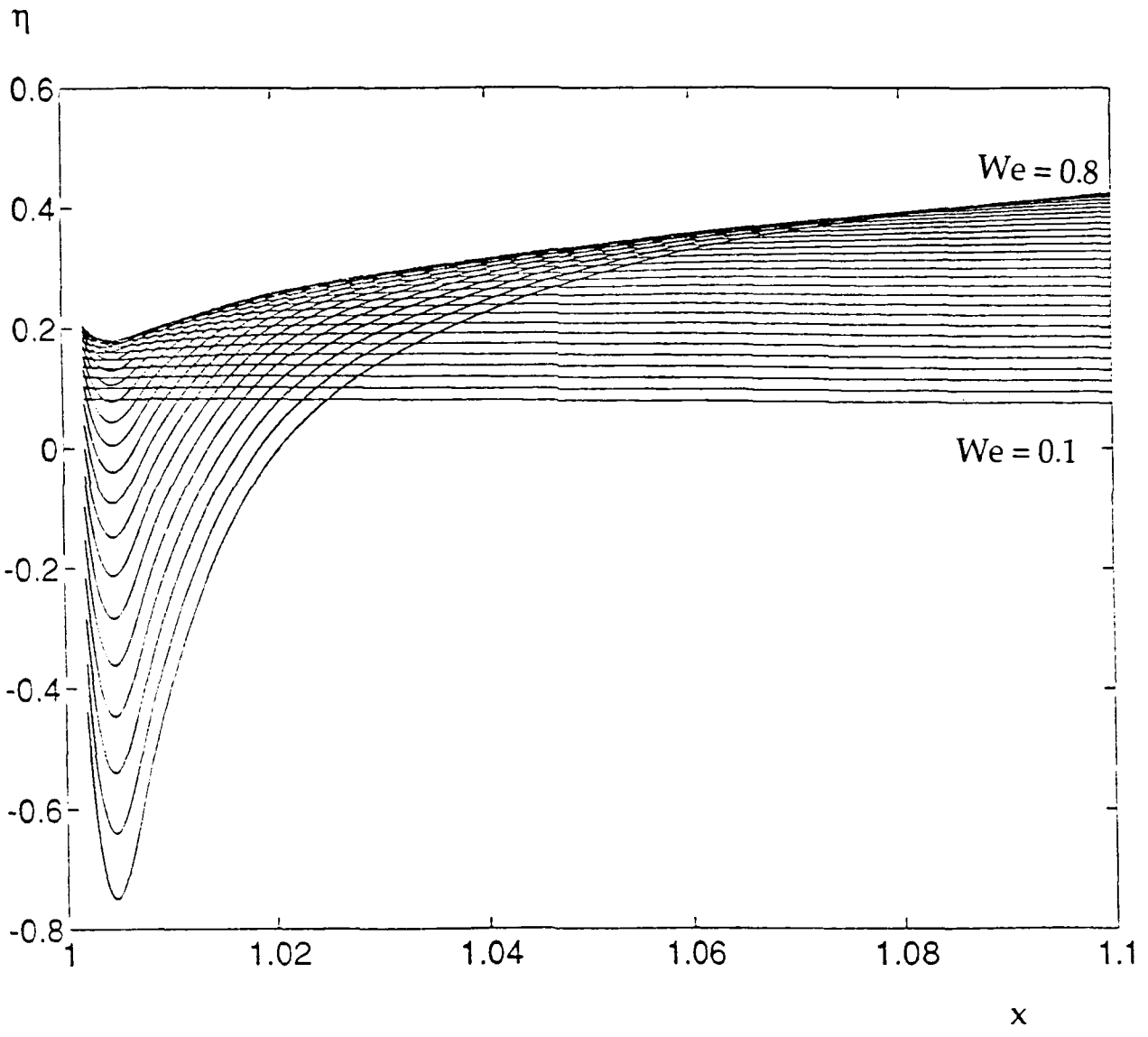

Figure 15 Shape of the interface for different Weber numbers(Bo=1)

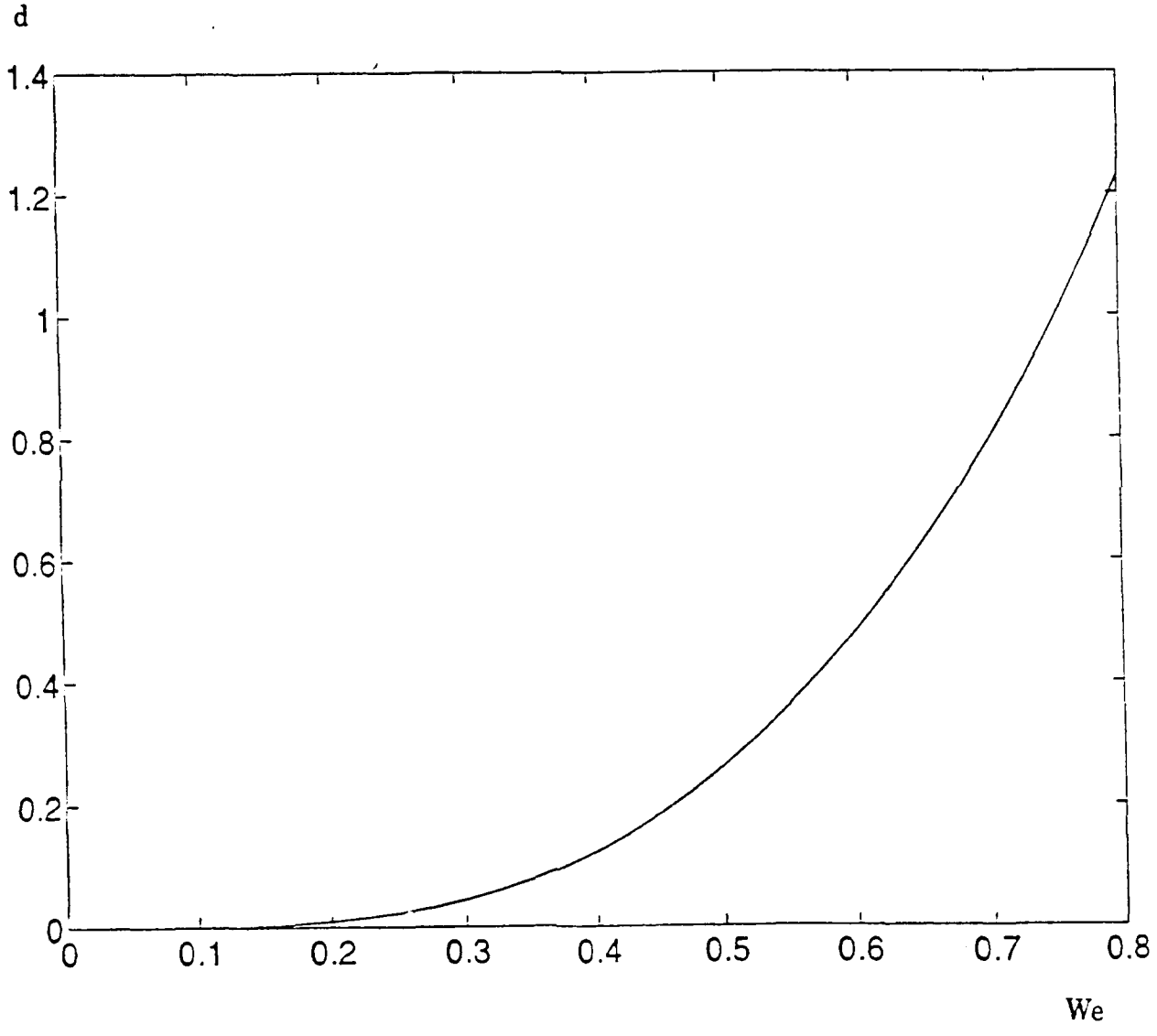

Figure 16 Gas gap depth d as a function of the Weber number (Bo=1).

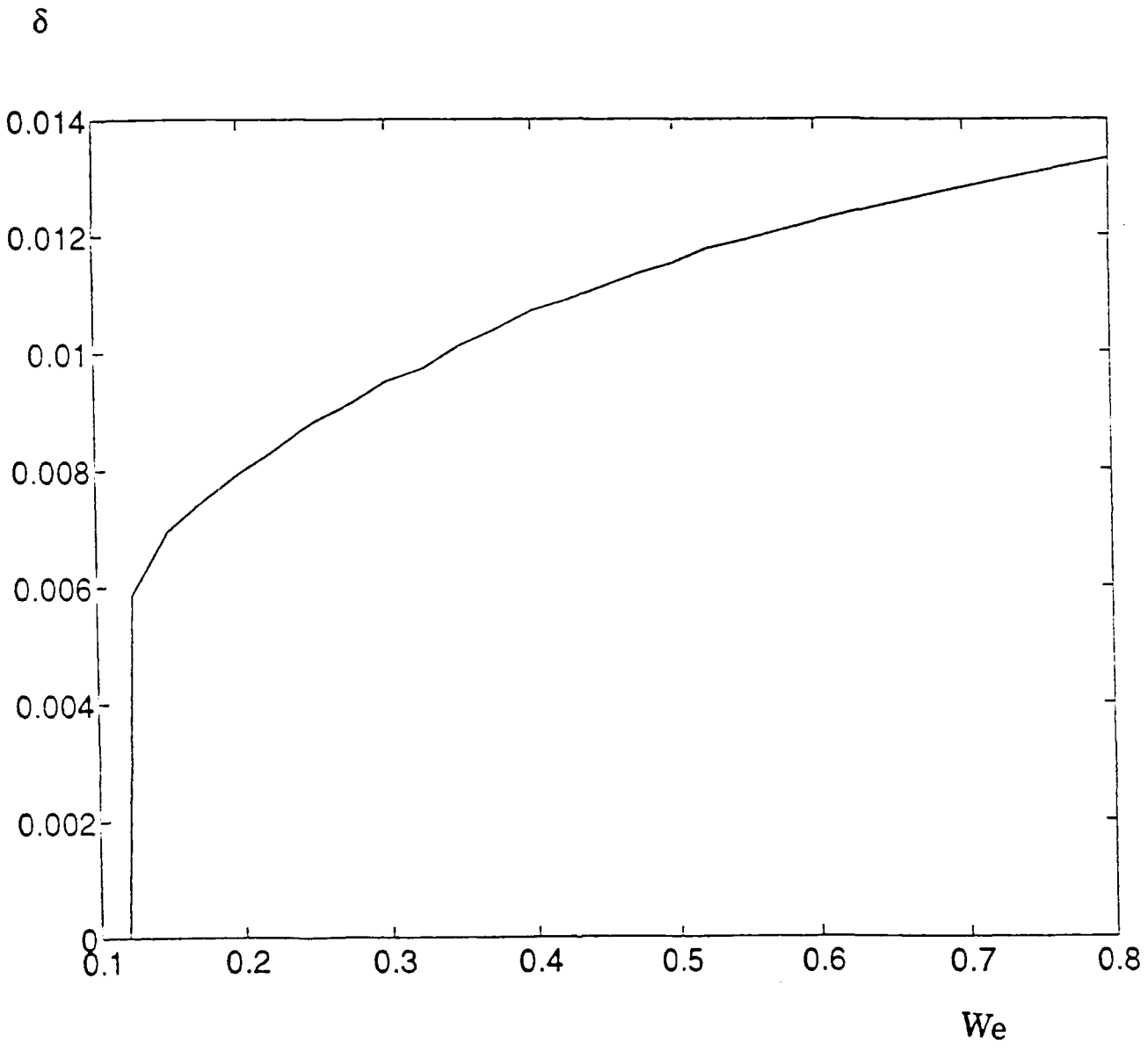

Figure 17 Gas gap width δ as a function of the Weber number (Bo=1)